AUTOMATIC CLASS LABELING OF CLASSIFIED IMAGERY USING A HYPERSPECTRAL LIBRARY

ILIA PARSHAKOV
Bachelor of Science, University of Lethbrsity, 2010

A Thesis
Submitted to the School of Graduate Studies
of the University of Lethbridge
in Partial Fulfilment of the
Requirements for the Degree

MASTER OF SCIENCE

Department of Geography
University of Lethbridge
LETHBRIDGE, ALBERTA, CANADA

ABSTRACT

Image classification is a fundamental information extraction procedure in remote sensing that is used in land-cover and land-use mapping. Despite being considered as a replacement for manual mapping, it still requires some degree of analyst intervention. This makes the process of image classification time consuming, subjective, and error prone. For example, in unsupervised classification, pixels are automatically grouped into classes, but the user has to manually label the classes as one land-cover type or another. As a general rule, the larger the number of classes, the more difficult it is to assign meaningful class labels. A fully automated post-classification procedure for class labeling was developed in an attempt to alleviate this problem. It labels spectral classes by matching their spectral characteristics with reference spectra. A Landsat TM image of an agricultural area was used for performance assessment. The algorithm was used to label a 20- and 100-class image generated by the ISODATA classifier. The 20-class image was used to compare the technique with the traditional manual labeling of classes, and the 100-class image was used to compare it with the Spectral Angle Mapper and Maximum Likelihood classifiers. The proposed technique produced a map that had an overall accuracy of 51%, outperforming the manual labeling (40% to 45% accuracy, depending on the analyst performing the labeling) and the Spectral Angle Mapper classifier (39%), but underperformed compared to the Maximum Likelihood technique (53% to 63%). The newly developed class-labeling algorithm provided better results for alfalfa, beans, corn, grass and sugar beet, whereas canola, corn, fallow, flax, potato, and wheat were identified with similar or lower accuracy, depending on the classifier it was compared with.

ACKNOWLEDGEMENTS

TABLE OF CONTENTS

LIST OF TABLES

LIST OF FIGURES

1   INTRODUCTION

1.1   Remote Sensing and Automation

Automated remote sensing techniques are required to meet various social, economic and scientific needs that demand constant generation of contemporary thematic maps. For example, land-cover and land-use mapping play an important role in monitoring biodiversity (Chapin *et al.,* 2000), biogeochemical cycles and climate change (Penner, 1994; Cihlar, 2000), as well as for the development of sustainable land-use strategies (Douglas, 1999). With its global coverage, remote sensing imaging presents an excellent tool for studying land-cover dynamics, an inexpensive and extremely powerful addition to traditional field observations and measurements.

One of the major issues in modern remote sensing is the lack of automated procedures that could help extract useful information from the tremendous amount of acquired data (Datcu *et al.,* 2002; Huang *et al.,* 2012; Huth *et al.*, 2012). There are numerous spaceborne and airborne sensors collecting petabytes (1 petabyte = 10^6 gigabytes) of data every day (ESA[1]; Behnkre *et al.,* 2005). Only a small portion of these data are actually used for the generation of information products.

Semi-automated image processing routines developed decades ago are still commonly used by remote sensing specialists (Ball and Hall, 1965; Tou and Gonzalez, 1977; Swain and Davis, 1978; Xie *et al.,* 2008). This has two important implications; first, it means that information extraction has to be performed by an expert in order to

---

[1] European Space Agency. Accessed on November 14, 2012:
http://www.esa.int/esaEO/SEM2F5JZBQE_index_0.html

produce accurate results (Huang *et al.,* 2012; Huth *et al.*, 2012), and secondly, involvement of human interaction makes the process of map production slow (Zha *et al.,* 2003; Lang *et al.,* 2008). Thus, there are petabytes of imagery on one side and a limited number of remote sensing analysts on the other. Automation of information extraction routines is the only way to eliminate this bottleneck (Datcu *et al.,* 2002; Huang *et al.,* 2012).

Various levels of government require accurate maps produced on a regular basis. For instance, the United States Department of Agriculture (USDA) mandates the production of new forest maps for the entire country every five years[2] and has long recognized the need for a national annual forest inventory program due to rapid changes in forest conditions (Van Deusen *et al.,* 1999; Gillespie, 1999). Generated maps not only have to meet certain quality standards, but also be consistent (Perry and Nelson, 2006). This requirement is difficult to achieve as experience and skill level vary from one analyst to another. In addition, it is impossible to evaluate the consistency of maps for areas where limited or no ground-reference data are available. This is especially true for countries with vast, relatively unexplored areas like Russia and Canada. The use of fully automated procedures will allow faster generation of maps of high consistency (Cihlar, 2000).

1.2   Remote Sensing Images

The study described in the thesis involved two types of remotely sensed data, multispectral and hyperspectral satellite imagery. Multispectral sensors are carefully

_____

[2] The Northeastern Forest Inventory and Analysis Program. Accessed on October 8, 2012: www.fs.fed.us/ne/fia/

designed to capture data in certain regions of the electromagnetic spectrum and have from three to several dozens of spectral bands (Colby *et al.,* 1978). Hyperspectral sensors acquire data in hundreds of narrow contiguous bands that can cover the entire solar reflective region (0.4 – 2.5 µm). Both types of data have a number of advantages and disadvantages. Multispectral and hyperspectral imaging differ in their historical coverage, temporal, spatial and spectral resolution.

Multispectral satellite imagery with global coverage has been available for more than four decades. In contrast, the first civilian hyperspectral sensor (Hyperion) was launched in space in year 2000. Thus, multispectral data provides a longer record of Earth observations from space, allowing to study long-term fluctuation in the distribution of various land-cover types.

The multispectral-data archive not only spans over a longer period of time, but is also more complete and almost continuous due to higher temporal resolution (revisit time), which is allowed by the larger geographic coverage of individual scenes. The data volume of a scene is determined by both its spatial and spectral components, which, along with technical constraints, restricts any particular system from having a high spatial and spectral resolution simultaneously. The lower spectral resolution of multispectral sensors allows them to have either a larger swath width (i.e., a larger spatial extend of a scene) or a narrower instantaneous field of view (i.e., a smaller pixel size). For the same reason, hyperspectral instruments cannot provide synoptic spatial coverage due to their narrow swath width.

The characteristics of the Hyperion hyperspectral and Landsat 5 TM and MODIS[3] multispectral sensors serve as a good illustration of the trade-off between spatial and spectral components of remotely sensed data. Both sensors have the same pixel size, but Hyperion has 242 spectral bands and a swath width of 7.6 km, whereas Landsat 5 TM has seven bands with a swath width of 185 km. MODIS has 36 spectral bands and a swath width of 2,330 km; depending on the spectral band, the spectral resolution of MODIS ranges from 250 m to 1,000 m.

The high spectral resolution of hyperspectral imagery provides a major advantage. Whereas multispectral sensors have a few broad spectral bands, hyperspectral imaging provides spectral resolution higher than that usually required by any particular application. For example, mineral mapping usually requires bands covering the 2000-nm to 2400-nm wavelength region that contains multiple molecular absorption features of minerals and mineral groups (Goetz *et al.*, 1983; Hook *et al.*, 1990), while the rest of the bands are simple not used. Spectral bands covering the near infrared and red-edge (680 nm – 750 nm) regions of the electromagnetic spectrum were to be more important for distinguishing vegetation types than any other region (Cochrane, 2000; Schmidt and Skidmore, 2003; Adam *et al.*, 2010). A multispectral sensor like ASTER[4] cannot resolve fine spectral features in these regions, resulting in lower identification accuracy (Koch *et al.*, 2005; Kruse *et al.*, 2009).

Finally, hyperspectral sensors have spectral bands at numerous atmospheric absorption features. These bands can be used, for example, to improve the atmospheric

---

[3] Moderate Resolution Imaging Spectroradiometer
[4] Advanced Spaceborne Thermal Emission and Reflection Radiometer

4

correction of the imagery (Goetz, 2009). In contrast, multispectral sensors acquire images only in atmospheric windows, forcing to use other ways to determine the path radiance (e.g., dark-object subtraction; Chavez, 1988).

1.3   Image Classification

Image classification is a fundamental information extraction procedure in remote sensing that is used for mapping land-use and land-cover types. Image classification started replacing manual mapping as soon as computers became available to the scientific community (Fu *et al.,* 1969; Phillips, 1973; Ballard and Eastwood, 1977). However, even nowadays, the human brain can perform certain mapping tasks better than computer programs thanks to the superior ability to interpret visual clues (Mas and Ramirez, 1996). Thus, image classification still requires some degree of analyst intervention, which makes the process of map creation time consuming and subjective (Lang *et al.,* 2008).

Commonly used image classification procedures can be divided into two main categories, supervised and unsupervised (Duda and Hart, 1973; Fleming and Hoffer, 1975; Lu and Weng, 2007). Supervised classification requires the analyst to select training areas. A training area is a polygon in an image that represents a particular land-cover or land-use type; they are thematic by definition. When training areas are selected, the computer gathers statistics on digital numbers (DN) of the pixels within the areas and then groups the remainder of the pixels in the image based on measures of statistical similarity to the training areas. Therefore, the quality of the resultant classification is determined by the ability of the analyst to select representative training sample areas (Campbell, 1981; Landgrebe, 2000).

In unsupervised classification, classes are produced automatically by grouping similar pixels into clusters based on their spectral characteristics. In a subsequent step, the user has to manually label the classes as one land-cover type or another. As a general rule, the larger the number of classes, the more difficult it is to assign meaningful class labels (Lang *et al.,* 2008). Depending on the number of land-cover types to be mapped and availability of ground-reference data, manual class labeling can be very subjective and error prone as the user is dependent on a variety of heuristics to arrive at a class-label decision. A fully automated procedure for the labeling of classes may produce more accurate and consistent maps and, therefore, can be used in mapping areas for which little or no ground-reference data are available.

Remote sensing image classification and particularly unsupervised classification of vegetation has a number of weaknesses. The problems that have to be addressed include the mismatch between spectral classes, land-cover types and land-use types; the classification of vegetation that constantly changes spectrally in both time and space; and the difficulty of classification quality assessment. These issues are discussed in the following sections.

1.4   Spectral Classes, Land-Cover Types, and Land-Use Types

Since image classification is mostly used in land-cover or land-use mapping (Foody, 2008), it is important to understand the difference between these concepts. Spectral classes are simply groups of pixels with similar spectral characteristics. If raw

digital numbers are converted into surface reflectance[5] prior to image classification, then spectral classes represent materials on the ground that are spectrally similar at the time of image acquisition. Land cover is the physical material that currently covers a certain portion of the ground, while land use, from the mapping perspective, is a patch of land with a certain socio-economic use (Fisher *et al.,* 2005).

Performing unsupervised classification, the user has to label spectral classes as land-cover or land-use types, even though these three concepts do not have a direct relationship. Appreciation of the complexity of this relationship helps to adequately assess the quality of image classification products. The user must understand that multiple land-cover types can be present in one spectral class or another. The same is true for land-use categories.

Because a specific land-cover type represents a single material, one may assume that its spectral properties are unique and stable (Duong, 2000). However, this is often not the case and remote sensing analysts should not rely on the assumption that classes in classified images depict unique land-cover types, and Comber at al. (2005) identified three main reasons why. First of all, it is often problematic to differentiate land-cover types based only on their spectral characteristics. High-spectral variability within land-cover types is typical for vegetation (Dennison and Roberts, 2003). For instance, variations in water availability, crop diseases and fertilizer leaching, among other factors, contribute to intra-class heterogeneity of crops (Fisher *et al.,* 2006).

---

[5] Spectral reflectance is the ratio of incident-to-reflected radiant flux. It is an inherent property of an object independent of the intensity of illumination (Peddle *et al.*, 2001).

On the other hand, different land-cover types can have similar characteristics (Townshend *et al.,* 1991; Liu *et al.,* 2003; Peña-Barragán *et al.,* 2011). This problem is particularly related to vegetation as all green plants have similar spectral properties (Williams and Hunt, 2002). Vegetation spectra are determined by leaf pigments, cell structure, water content, and plant structure, which are similar among different species of plants (Gates *et al.,* 1965).

Secondly, identification of land-cover types is increasingly erroneous with decreasing spatial resolution of the imagery. A spatially "large" pixel may overlay a mixture of land-cover types and be identified as a land cover that is not even present in the pixel. This problem is known as the mixed-pixel effect (Prager, 1980). Besides, pixels with the same vegetation type but different plant density (biomass) will be spectrally different and can be classified as different classes (Duong, 2000).

Thirdly, patch size (the area of the land-cover patch in which the classified pixel is located) and land-cover heterogeneity also have effects on classification accuracy. Land-cover heterogeneity can be measured as the number of land-cover categories occurring in a window of a certain size (e.g., 3×3 pixels). The bigger the patch size and the smaller the spatial heterogeneity, the higher is the probability that the pixel is classified correctly (Smith, 2003).

1.5   Vegetation Phenology

Identification of vegetation land-cover types in remote sensing imagery is also complicated by temporal changes in reflectance characteristics. Throughout the year, plants undergo physiological and structural changes that affect their reflectance (Price, 1994). For example, changes in the concentration of chlorophyll and other pigments alter

8

the absorption of radiant energy in the visible region of the electromagnetic spectrum. Seasonal variations in cell structure and canopy architecture affect the reflectance in the near infrared, while the reflectance in the short-wave infrared is mainly influenced by changes in leaf water content. Due to these reasons, remote sensing analysts who classify vegetation must have good knowledge of plant phenology.

Many authors, such as Draeger *et al.* (1971), Ballard and Eastwood (1977), Brisco and Brown (1995), Lunetta and Balogh (1999), Oetter *et al.* (2000), Guerschman *et al.* (2003), Tottrup (2004), Blaes *et al.* (2005) and Lu and Weng (2007), recommended the incorporation of crop phenology in the classification process in order to achieve higher accuracy. For example, Peña-Barragán (2011) achieved a much higher overall accuracy (79%) classifying crops by using a three-period approach (mid-spring, early-summer and late-summer) in comparison to two-period approaches (from 64% to 73%, depending on which two periods were used). The author concluded that using a combination of mid-spring and late-summer imagery provided better classification accuracy of permanent crops (alfalfa, vineyard, almond and walnut); early-summer and late-summer imagery yielded the best classification accuracy of summer crops (corn, rice, safflower, sunflower and tomato); and mid-spring and early-summer imagery contained more useful information for the discrimination of winter cereals (oat, rye and wheat). Draeger *et al.* (1971) found that barley and wheat can be easily differentiated in May images, but are indistinguishable in mid-summer images.

However, reflectance characteristics change throughout the crop growing season not necessarily as a function of date (time of the year), but as a function of crop maturity (Haralick *et al.,* 1980). Differences in farmer decisions and local weather can result in

different crop development schedules and crop patterns. Some crops, such as alfalfa and hay, are influenced by the cutting schedule, resulting in high spatial and temporal variability (Putnam *et al.,* 2007). Thus, fields of the same crop type can have very different spectral characteristics within a scene.

1.6   Spectral library

The reference spectra of different materials, often referred to as endmembers or spectral signatures, can be used to identify these materials in remote sensing imagery. Spectral signatures are either recorded on the ground using a spectroradiometer or extracted from airborne or spaceborne data. Spectral signatures are stored in spectral libraries, which can range in complexity from simple collections of spectra to complex databases with a hierarchical structure.

Very few spectral libraries are open and easily accessible. Among such libraries are the USGS (United States Geological Survey) Spectral Library (Clark *et al.,* 2007) and the ASU (Arizona State University) Spectral Library[6] (Christensen *et al.,* 2000). These libraries include mostly spectra of rocks, minerals and soils, but very few vegetation spectra. Therefore, it might be difficult to find appropriate spectral signatures, especially for highly dynamic vegetation land-cover types.

Unable to find needed spectra in existing online libraries, many authors develop their own spectral libraries (e.g., Roberts *et al.,* 1998; Girouard *et al.,* 2004; Herold *et al.,* 2004). A database like SPECCHIO (Spectral Input/Output; Bojinski *et al.*, 2003; Hueni *et al.*, 2009) can be used to store spectra and related metadata (i.e., information about the

---

[6] ASU (Arizona State University) Spectral Library. Accessed on December 29, 2012: http://speclib.asu.edu/

spectra) in an organized fashion. Besides storing spectral signatures, the database provides tools for querying and even analysis of data. The functionality of the database software is being extended through regular updates.

1.7   Objectives

The aim of this study was to develop an automated procedure that labels spectral classes automatically based on the information contained in a spectral library. A spectral library for the land-cover types present in the study was developed and tested on sample imagery to assess the efficacy of the automated spectral labeling procedure that utilized a measure of spectral variability as the assignment rule for estimating group membership.

1.8   Hypothesis

If remote sensing is useful at distinguishing scene components based on the spectral information, then with the assistance of an automated spectral library function, it should be possible to develop an algorithm that reliably achieves similar or higher classification accuracies in comparison to manual techniques. The main advantage of semi-automated classification methods is that they combine the processing power of the computer with the capability of the human brain to use visual clues. That is, if there are no visual clues for an analyst to use, the accuracy will depend only on the suitability of the classification algorithm and the quality of ground-reference data used for selecting training areas or labeling classes. This is the case for this study, in which a Landsat 5 TM image is used to classify agricultural crops. For the analyst's eye, crop fields often look too much alike to distinguish at the Landsat 5 TM spatial resolution.

Therefore, the hypothesis is that, in a Landsat image, an automated procedure will label classes better than a human interpreter because it can more fully exploit the spectral component of the data.

1.9   Thesis Structure

This chapter has discussed why the lack of automated procedures is one of the major issues in remote sensing today, why it is so difficult to map vegetation land-cover types using remote sensing image data, and why the accuracy assessment of image classification is still not standardized. Chapter 2 reviews the literature and gives a few examples of existing approaches to the automation of image classification. Chapter 3 describes the methodology of the proposed approach to automation based on automated class labeling. Accuracy and performance assessment results are described in Chapter 4 and discussed in Chapter 5. This is followed by the concluding remarks and recommendations for further research in Chapter 6.

2   BACKGROUND

Many attempts have been made towards the automation of image classification in remote sensing. The goal has always been to make the image classification process faster, more accurate, and less subjective (McCaffrey and Franklin, 1993; Cihlar, 2000). Many approaches to automation exist; they range from decision tree algorithms to signature extension and automatic class labeling procedures. However, they all have their drawbacks that prevent them from being universally adopted by remote sensing specialists.

This chapter will start by discussing two popular semi-automated classifiers and then review existing automated procedures. A particular attention will be given to automatic techniques that use spectral matching algorithms to label image pixels as they are most related to the method presented in the thesis.

2.1   Traditional Semi-Automated Classification Methods

Maximum Likelihood and Iterative Self-Organizing Data Analysis Technique (ISODATA) are two notable examples of supervised and unsupervised classifiers, respectively. Neither of these techniques is fully automated, but their inclusion in this chapter is justified by the fact that many automated routines, including the one presented in the thesis, are built upon them.

2.1.1   Maximum Likelihood Supervised Classifier

In supervised classification, the user selects polygons (training areas) in the image representing particular land-cover types, and then the classifier assigns each pixel to a

land-cover type with which it has the highest similarity (Section 1.3). This provides a major advantage, because training areas by definition represent thematic classes (i.e., land-cover types). For this reason, resultant maps should theoretically confirm better with the actual distribution of land-cover types.

The Maximum Likelihood technique was described in 1978 (Swain and Davis, 1978) and has been one of the most widely used supervised classification methods since then (Foody *et al.,* 1992; Shafri *et al.,* 2007; Govender *et al*, 2007; Xie *et al.,* 2008). The maximum likelihood classification algorithm uses the multivariate normal distribution statistical theory, and in terms of statistics, similarity is calculated as the probability that a given pixel belongs to a particular class (Swain and Davis, 1978; Lillesand and Kiefer, 2002). Figure 2.1 shows an example in which a pixel is assigned to a class. In this case, the pixel is allocated to class 3 due to the highest probability of that class.
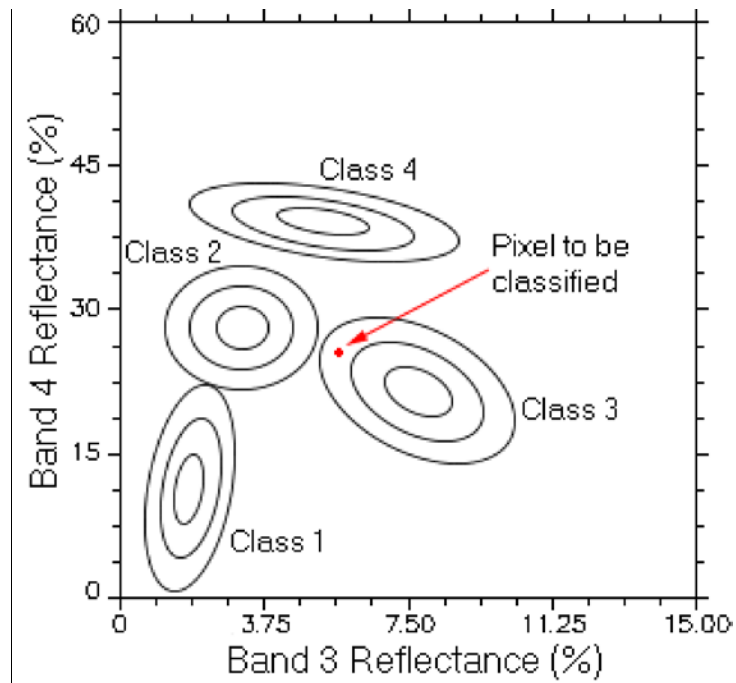
Figure 2.1: Equiprobability contours (ellipses) for four classes. Smaller ellipses indicate higher probability.

14

The main disadvantage of the method is associated with the fact that it is based on the assumption that classes have a normal distribution, although many land-cover types have multimodal distribution of reflectance as discussed in Chapter 1.

Even nowadays, the Maximum Likelihood classifier can provide similar or better results in comparison to more recent supervised classification methods, such as Neural Network or Support Vector Machine (Pal and Mather, 2005; Waske and Benediktsson, 2007; Shafri *et al.,* 2007). Many remote sensing specialists prefer to use this technique, because it is readily available and has a fast processing time (Pal and Mather, 2005). Another advantage of this classifier is that it takes into account the covariance of the data, unlike some other commonly used classifiers (Ozesmi and Bauer, 2002).

2.1.2   ISODATA Unsupervised Classifier

The ISODATA clustering algorithm is one of the most popular unsupervised classifiers (Ball and Hall, 1965; Tou and Gonzalez, 1977; Xie *et al.,* 2008). It uses an iterative process through which it reclusters pixels until it finds groups that are most separable from one another in spectral space and are relatively homogeneous. During the first iteration, the algorithm assigns arbitrary initial cluster means that are evenly distributed in the data space. Pixels are allocated to clusters using the minimum distance to mean approach (Ball and Hall, 1965).

Each iteration cluster means are re-calculated and pixels are reclassified to minimize the average Euclidian distance between the pixels and corresponding (nearest) cluster means (Figure 2.2). The reclustering process is terminated when the change between two consequent iterations becomes smaller than the selected threshold or when

the maximum number of iterations is reached. Clusters can be merged and split based on user specified criteria (e.g., minimum number of pixels in a class, maximum class standard deviation, or minimum distance between classes)[7].

Clusters are merged if either the number of members (pixel) in a cluster is less than a certain threshold or if the centers of two clusters are closer than a certain threshold. Clusters are split into two different clusters if the cluster standard deviation exceeds a predefined value and the number of members (pixels) is twice the threshold for the minimum number of members.
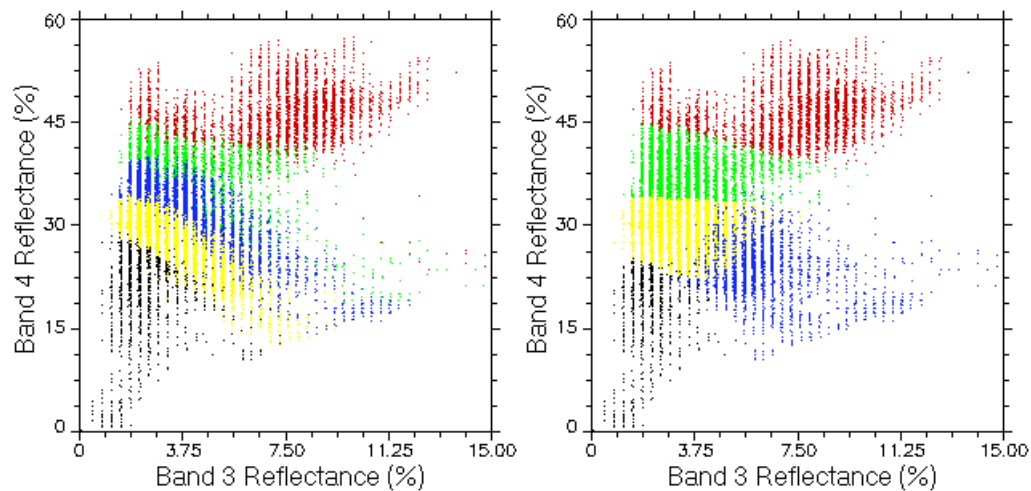
Figure 2.2: Scatter plots for five clusters after 1 (left) and 50 (right) ISODATA iterations. After 50 iterations, the clusters are more compact and contain pixels that are more spectrally similar to each other.

Thus, unsupervised classifiers group image pixels automatically, but the user has to manually label resultant classes. Manual class labeling can be a very subjective and time consuming process. In fact, it can be more time consuming than the selection of training areas in supervised classification (personal experience).

---

[7] ENVI Tutorial: Classification Methods. Accessed on January 3, 2013:
http://www.exelisvis.com/portals/0/tutorials/envi/Classification_Methods.pdf

16

One of the major disadvantages of unsupervised methods is that the classification process is performed by a computer algorithm that does not try to identify land-cover types but rather finds natural (from a statistical point of view) groupings of pixels. Image classification is often a per-pixel operation, which is based only on the spectral component of the data; the spatial component is ignored. For this reason, as this study will show, the mismatch in spatial distribution between resultant spectral classes and actual land-cover types can be substantial, which results in a lower map accuracy.

A number of authors (Kelly and White, 1993; Driese *et al.,* 1997; Homer *et al.,* 1997; Vogelmann *et al.,* 1998; Cihlar, 2000) advocate for the use of the hyperclustering approach (producing a large quantity of clusters) to mitigate the aforementioned problem. When the number of generated clusters is small (i.e., comparable with the amount of thematic classes in the scene), the mismatch between spectral classes and land-cover types can be quite large. In this case, one cluster may contain several thematic classes and vice versa. However, if the number of clusters is much greater than the number of land-cover types, it is more certain that spectral classes do not contain multiple thematic classes. These "pure" spectral classes can then be merged together to produce a more accurate map in a more desirable form.

The hyperclustering approach should be especially beneficial when the subject of classification is vegetation (Driese *et al.,* 1997; Homer *et al.,* 1997; Vogelmann *et al.,* 1998). Vegetation land-cover types often have a multimodal reflectance distribution due to the high within-class spectral variability (Section 1.4). A higher level of accuracy can be achieved if the classifier is set to produce a number of spectral classes comparable not to the number of land-cover types, but the number of subtypes that have unimodal

reflectance distribution. As the latter is often unknown, it is safe to produce a very large quantity of clusters.

Although the benefits of generating more clusters with consequent merging was discovered in early years of satellite image classification, it was also found that the manual labeling of a large number of clusters can be extremely difficult without sufficient ground-reference data (Fleming and Hoffer, 1975).

2.2   Existing automated classification techniques

Several automated techniques were chosen to illustrate the variety of existing approaches to the automation of image classification. Some of these methods present extensions to conventional supervised (e.g., techniques based on signature extension and training area reuse) or unsupervised (e.g., the data assisted class labeling routine) classifiers, or both (various hybrid procedures), while others (e.g., decision tree or spectral matching classifiers) are self-contained.

2.2.1   Decision Tree Classification Algorithms

The decision tree is an approach where pixels are classified based on a sequence of binary decisions (Safavian and Landgrebe, 1991). Depending on the decision, the first conditional statement leads to the second, the second to the third and so on (

Figure 2.3). The main advantages of this method are computational efficiency, simplicity (easy to interpret), and the capability of operating with both numeric and categorical data (Friedl and Brodley, 1997). However, substantial expert knowledge is required to create a decision tree. Another disadvantage of this approach is that it is often restricted to only one type of data. For example, a decision tree constructed to classify

Landsat TM images might not be able to classify SPOT HRV images with the same accuracy, because the latter has fewer bands and they do not cover exactly the same regions of the electromagnetic spectrum.
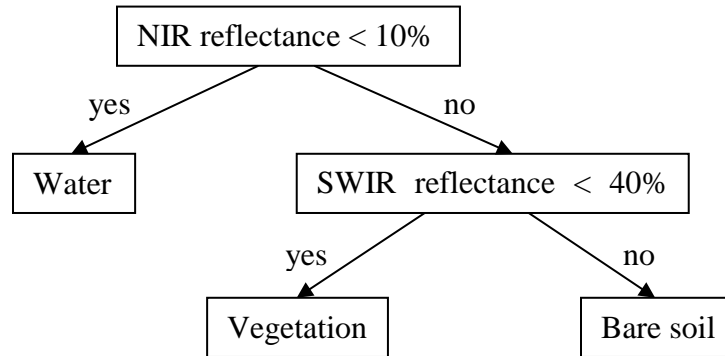
Figure 2.3: A simple decision tree classification scheme that classifies image pixels into three classes: bare soil, water, and vegetation. The diagram is for demonstration purposes only.

2.2.2   Hybrid Procedures and Region Growing

Hybrid procedures combine the advantages of both supervised and unsupervised techniques to overcome the drawbacks of each and/or reduce the human factor (Scrivani *et al.,* 2001; Serra *et al.,* 2005; Musy *et al.,* 2006). For example, the first step of a hybrid procedure can be the generation of training samples by region growing from seed points of known land-cover types. Unsupervised classification is then performed, and each produced spectral cluster is assigned to a specific thematic class if the corresponding training sample contains pixels of the cluster (Scrivani *et al.* 2001; Musy *et al.,* 2006).

If the pixels of a cluster are found in training areas representing different classes, the cluster is marked as "impure" and undergoes reclustering. This step is repeated until all the clusters are assigned to thematic classes or a user-specified maximum number of iterations is achieved. Unlike in some supervised classification approaches, it is not required that a training sample area represents a spectral class that is normally distributed

19

and clearly distinct from other spectral classes (Musy *et al.,* 2006). In contrast to a traditional unsupervised classification, clusters are labeled automatically and higher accuracy is achieved by re-clustering (Scrivani *et al.* 2001; Musy *et al.,* 2006). However, field work or very high-resolution reference imagery is required to obtain seed points (Musy *et al.,* 2006).

2.2.3 Signature Extension and Training Area Reuse

Another approach to automation is based on utilizing the common information shared by multiple images (e.g., multi-temporal images). In this case, one image in a series is classified using a supervised technique and either the signatures of the generated classes (Olthof *et al.,* 2005) or the locations of the training samples (Cazes *et al.,* 2004) are extended to the other images in the series. Both ways require manual selection of training areas in at least one of the images.

In addition, the signature extension approach has one more substantial disadvantage. The radiation reflected from the target is severely altered by water vapour and other gases and particles in the atmosphere before it arrives at the sensor. Because of different weather conditions, the atmosphere absorbs and scatters radiation differently depending on the time and location of image data acquisition. Therefore, the signature extension method requires a very accurate atmospheric correction or relative normalization (Olthof *et al.,* 2005).

2.2.4 Data Assisted Class Labeling

A procedure similar to the one proposed in the thesis was developed by Lang *et al.* (2008). In this procedure, an algorithm was used to label each of an excessive number

of spectral classes as one of the four land-cover types: forest, agriculture, urban, and water. Spectral classes were generated by the ISODATA unsupervised classifier. High-spatial resolution ortho-photographs were used for reference purposes to obtain two sets of sample points from Landsat TM and ETM+ images of the same area acquired during separate growing seasons (summer and fall). These two sets were named Reference Data 1 and 2. The former was used for automatic labeling of spectral classes while the latter was used for accuracy assessment. The labeling was based on the majority rule. For example, if a spectral class contains 60 reference points representing agriculture, 10 points representing forest, and 5 points representing water, the class is labeled as "Agriculture".

Lang *et al.* (2008) compared the performance of this technique with the performance of the following three commonly used conventional methods: ISODATA, minimum distance, and maximum-likelihood classifications. It was found that the accuracy of the maps produced with the help of the labeling algorithm was better than the accuracy of the maps produced using the three conventional classification methods.

The advantage of the method is that it is simple and produces relatively "pure" classes. The latter is achieved by utilizing the advantages of the hyperclustering approach, which requires the generation of large amount of classes (Section 2.1.2). The disadvantage is the need for reference data.

2.3   Automatic Classifiers Based on Spectral Matching Techniques

Some classifiers use spectral matching algorithms to cluster image pixels. They group pixels based on spectral similarity to reference spectra. Reference spectra are

usually represented by the spectral signatures of the land-cover types of interest. Reference data are first resampled to match the spectral characteristics of the image data to be classified and then compared to the spectrum of each pixel. Many different algorithms are used to perform spectral matching, including the Euclidean Distance (the distance between the reference and pixel spectra is calculated in an n-dimensional space, where n is the number of bands; Van der Meer, 2006), Spectral Feature Fitting, Correlation Similarity Measure, and Spectral Angle Mapper.

Spectral Feature Fitting is a spectral matching technique that first normalizes and enhances spectral features by removing the continuum from the reflectance spectra and then compares individual absorption features using the least-squares fitting method (Figure 2.4; Clark *et al.,* 1990; Kokaly *et al.,* 2003; Van der Meer, 2004).
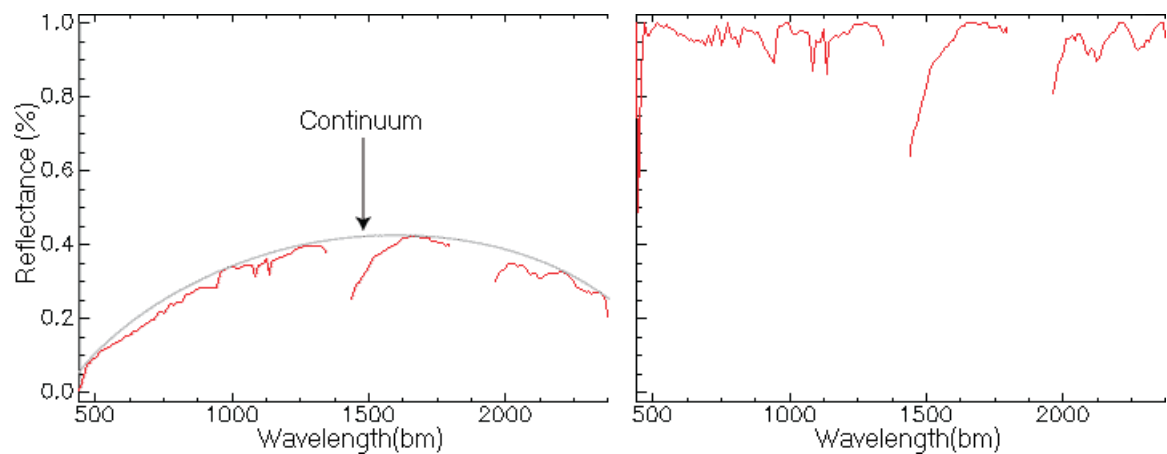
Figure 2.4: Original spectrum and its continuum (left) and continuum-removed spectrum (right).

The Spectral Angle Mapper (SAM) matches spectra by finding the smallest angle between the vectors representing the reference spectrum and spectrum to be matched in an n-dimensional space, where n is the number of bands (Kruse, 1993). Figure 2.5 shows the angle (θ) between two 3-band spectra.

22
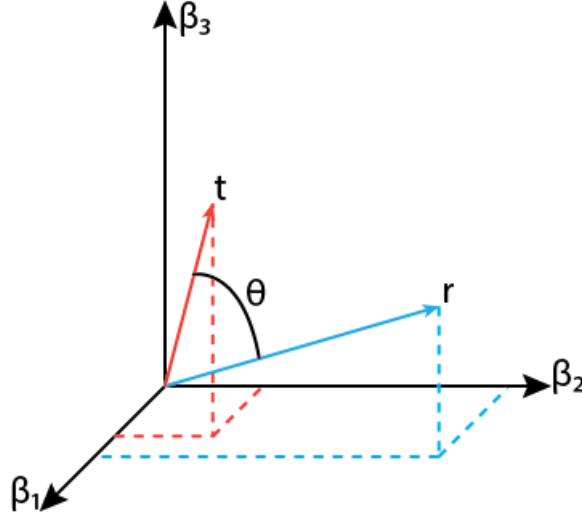
Figure 2.5: The angle (θ) between the reference spectrum (r) and the spectrum to be matched (t). The spectra have three bands (β1, β2, β3). The origin corresponds to zero reflectance in all three bands.

The angle is calculated using the following equation:

$$SAM = \cos^{-1}\left(\frac{\sum_{b=1}^{n} t_b r_b}{\sqrt{\sum_{b=1}^{n} t_b^2 \sum_{b=1}^{n} r_b^2}}\right),$$ [3.1]

where **n** is the number of bands, $\mathbf{r_b}$ and $\mathbf{t_b}$ are the amplitudes of the reference spectrum and the spectrum to be matched in band **b**, respectively. The value of 0 represents the closest match possible.

The *Correlation Similarity Measure* (CSM) can also be used to find similar spectra. Staenz *et al.* (1999) found that it outperformed the SAM (83% against 77% of pixels correctly classified as barley, beans, canola and wheat using *casi*[8] data), as well as two other techniques (Chi-square: 72% and Square Error Statistics: 68%). This technique is based on the Pearson correlation coefficient (Snedecor and Cochran, 1967). While both

---

[8] Compact Airborne Spectrographic Imager

SAM and CSM are insensitive to the reflectance amplitude, CSM differs from SAM in that it is centralized in the mean of r and t spectra. This standardizes the data, which makes the method more suitable for some applications (Staenz *et al.,* 1999; de Carvalho and Meneses, 2000). The CSM is calculated using the following formula:

$$CSM = \left(\frac{\sum_{b=1}^{n} t_b r_b - n\bar{t}\bar{r}}{(n-1)\sigma_t \sigma_r}\right)^2 , \qquad\qquad [3.2]$$

where $\bar{r}$ and $\bar{t}$ are the mean amplitudes and σ_r and σ_t are the standard deviations of the reference spectrum and the spectrum to be matched, respectively. CSM ranges from 0 to 1 where 1 indicates a perfect match.

The benefits of using spectral matching classifiers are low computational cost and no necessity for ground-reference data. On the other hand, these techniques assume that pixel values represent surface reflectance and, therefore, require very careful image preprocessing. This requirement limits the accuracy of resultant maps, because it is not possible to estimate surface reflectance from raw pixel values with 100% accuracy due to atmospheric effects, calibration errors, and sensor artifacts.

Another challenge is to find appropriate spectral signatures. As mentioned in Section 1.6, there are very few vegetation spectral signatures that are openly available. The users of spectral matching techniques usually have to create their own spectral libraries from scratch, unless they are pursuing a mineral mapping application (Dennison et al, 2004; Rao *et al.*, 2007; Cho *et al.*, 2010).

2.4   Classification Accuracy Assessment

Accuracy assessment is used to evaluate the quality of maps resulting from classified imagery or, in other words, the usefulness of these maps to their users. It allows to estimate what portion of the area occupied by a particular land-cover/land-use type was identified correctly in a classified image (e.g., wheat identified as wheat). Map accuracy is determined by calculating how closely the map conforms to available ground-reference data.

Since the publication of "Land-use Classification Schemes" by Anderson (1971), many authors adopted 85% as the overall-accuracy target. Anderson used Landsat 1 Multispectral Scanner System (MSS) images for the mapping of broad land-cover types, such as urban, agriculture, forest, and water, at small scales (1:250,000 – 1:1,200,000). Scepan (1999) adopted the same target accuracy to assess the quality of the broad land-cover classification of 1-km spatial resolution NOAA AVHRR imagery. McCormick (1999) also used the 85-% threshold in a completely different study using narrow, sub-species classes and high-spatial-resolution aerial photography.

Foody (2008) argues that studies like these differ too greatly to accept the same accuracy target and that a realistic target should be defined for each particular mapping application depending on scale, nature of classes (e.g., narrow or broad land-cover categories), spatial and spectral resolution of the imagery, and time of acquisition. Congalton (1991) adds a few other factors: ground data collection, classification scheme, spatial autocorrelation, sample size, and sampling scheme. For example, the classification of crop fields can yield an overall accuracy of less than 60% for a single-date

25

multispectral image and up to 90% for multi-temporal multi-sensor imagery (Ban, 2003; Eckert and Kneubühler, 2004; Blaes *et al.*, 2005; Leite *et al.*, 2008). Therefore, no single classification accuracy target can possibly be universally adopted (Fisher *et al.,* 2005; Foody, 2008; Congalton and Green, 2009).

3   METHODS

3.1   Study Area

The study site is an agricultural area near Lethbridge, Southern Alberta (49°44'N, 112°34'W). It is located in the moist mixed grassland ecoregion (prairies ecozone). This ecoregion has semi-arid moisture conditions, warm summers, strong winds, and low to moderate precipitation, determining the need for irrigation; the dominant soil type is Dark Brown Chernozemic[9]. According to the reports by the Alberta Agriculture and Rural Development (AARD) for June 23, 2005, some crop fields in the area were damaged by flooding, hailstorms, leaf diseases, and fertilizer leaching[10].

Most farmers in this region use the center pivot irrigation system. The majority of the crop fields are the same size of about 0.65 km^2, determined by the length of the irrigation equipment rotating around the pivot. Accordingly, there are approximately 600 crop fields in the test image.

3.2   Data

Landsat 5 TM, EO-1 Hyperion, and ground-reference data for the study site were provided by the Agriculture and Agri-Food Canada (AAFC). The image data were acquired on July 2 (Hyperion) and July 3 (Landsat) of 2005. Two Landsat images were mosaicked using the latitude/longitude information of the data sets to cover the study site. A subset of the resultant mosaic was used to test the method (Figure 3.1). The study site covers an area of about 430 km^2.

---

[9] The Moist Mixed Grassland Ecoregion. Alberta Agriculture and Rural Development. Accessed on November 15, 2012: http://www1.agric.gov.ab.ca/$department/deptdocs.nsf/all/sag3411
[10] Crop Conditions as of June 23, 2005. Alberta Agriculture and Rural Development. Accessed on October 6, 2012: http://www1.agric.gov.ab.ca/$department/deptdocs.nsf/all/sdd10016
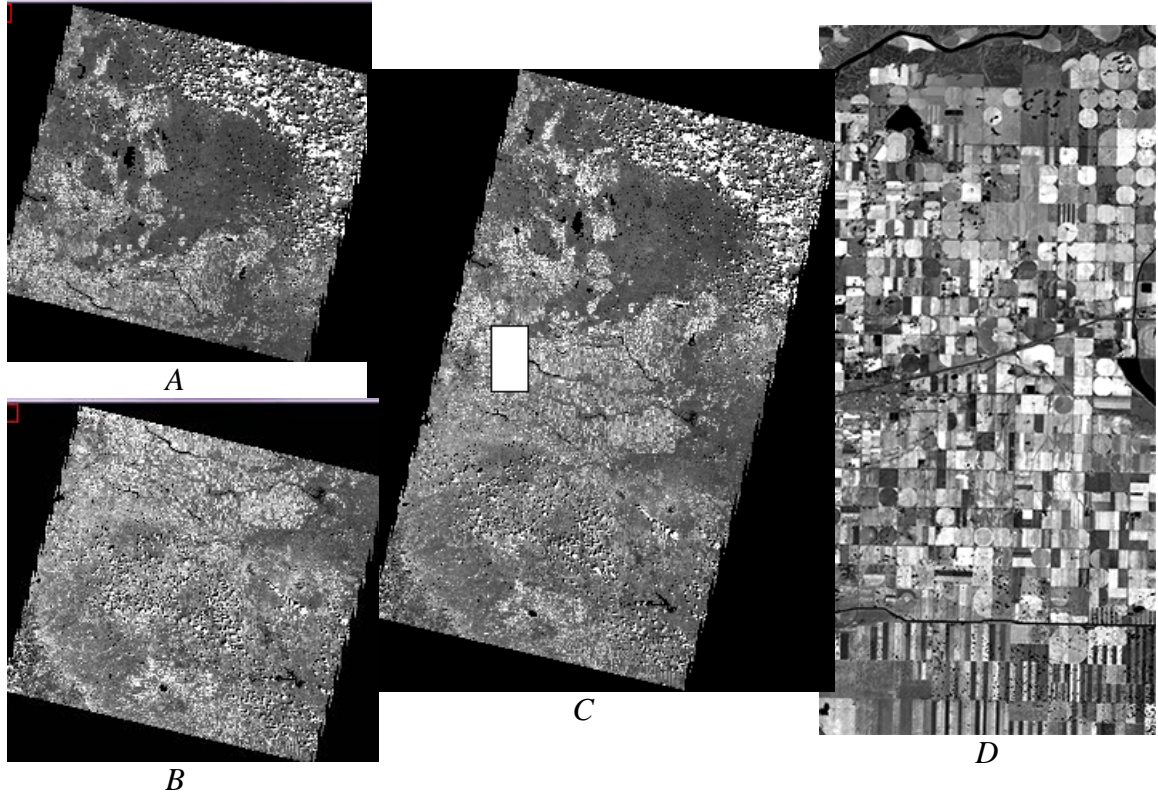
Figure 3.1: Two Landsat 5 TM images (A and B) were mosaicked (C) and a subset of the mosaic (D) was used in the study. The white rectangle in image C represents the study area (D) for which ground-reference data were provided.

Ground-reference data collected through a field survey provided crop type information for 53 fields and 11 different crop types. The latter are alfalfa (*Medicago sativa* L.), barley (*Hordeum vulgare* L.), beans (*Phaseolus vulgaris* L.), canola (*Brassica napus* L.), corn (*Zea mays* L.), flax (*Linum usitatissimum* L.), grass (mixed grass species), potato (*Solanum tuberosum* L.), sugar beet (*Beta vulgaris* L.), wheat (*Triticum aestivum* L.), and fallow. A few other, non-agricultural land-cover types are present in the image, including uncultivated grassland, roads, and water.

3.3   Sensor Characteristics

Any multispectral and hyperspectral data can be used as input. In the case of this study, classification was performed using multispectral Landsat 5 TM image data,

whereas the spectral signatures of the land-cover types were extracted from the hyperspectral Hyperion data. The characteristics of the sensors are listed in Table 3.1.

Table 3.1: Landsat 5 TM and Hyperion sensor characteristics.

	Landsat 5 TM			Hyperion
Spectral Resolution	Band	Wavelength, μm	Description	242 contiguous bands from 0.350 to 2.582 μm with a 10-nm bandwidth. Bands 1 − 7, 58 − 76, and 221 − 242 are zero bands*; therefore, the actual spectral coverage is 0.421 to 2.401 μm.
	1	0.45-0.52	Blue	
	2	0.53-0.61	Green	
	3	0.63-0.69	Red	
	4	0.78-0.90	Near Infrared (IR)	
	5	1.55-1.75	Short-wave IR	
	6	10.4-12.5	Thermal IR	
	7	2.09-2.35	Short-wave IR	
Spatial Resolution	30 m (120 m for band 6)			30 m
Orbit	Circular, sun-synchronous, near-polar orbit at an altitude of 705 km			
Equatorial Crossing	9:45 a.m. +/- 15 minutes			10:00 a.m. +/- 15 minutes
Revisit Time	16 days			16 days
Swath Width	185 km			7.6 km
Inclination	98.2°			98.2°
Radiometric Resolution	8 bit			16 bit
Launch Year	1984			2000
Level of Correction	Level 1T (geometrically and radiometrically corrected)			Level 1R (radiometrically corrected) or Level 1Gst (geometrically and radiometrically corrected)
Cost	Free			Free
Signal to Noise Ratio	Less than 100:1 (Mitchell and Glenn, 2009)			≈150:1 (visible), ≈100:1 (near IR), ≈50:1 (short-wave IR) (Pearlman *et al.,* 2003)

* These bands contain no data as they were not calibrated due to insufficient signal (Barry, 2001).

Landsat 5 Thematic Mapper (TM) is a multispectral across-track scanner. In this type of sensor, a mirror scans across-track, acquiring several lines of data. Landsat 5 TM

acquires sixteen lines in bands 1 – 5 and 7 per each scan, and an oscillating mirror allows scanning in both directions.

The disadvantage of using an oscillating mirror is the requirement for another set of rotating mirrors called the scan-line corrector. Due to the presence of moving parts, this type of sensors are more prone to wearing out. For example, the scan-line corrector of Landsat 7 ETM+ (Enhanced Thematic Mapper Plus) failed four years after the satellite was launched in 1999, which caused (and is causing) wedge-shaped gaps on each side of the acquired images. That is why Landsat 5 TM imagery was preferred over Landsat 7 ETM+ images. Launched in 1984, Landsat 5 TM is only now being decommissioned[11]. It was still operational up until recently, although its characteristics changed because of aging. In particular, the sensor's internal calibrator degraded through time. Nonetheless, accurate radiometric calibration of later imagery is still possible due to cross-calibration with Landsat 7 ETM+ and vicarious measurements (Chander and Markham, 2003).

The Landsat TM sensors were designed to maximize the capability of discriminating vegetation types at a limited spectral resolution (Colby *et al.,* 1978; Figure 3.2). The bands cover wavelength regions important for measuring absorption features, such as those caused by leaf pigments, cell structure and water content (Rahman *et al.,* 2004). Some authors (Mitchell and Glenn, 2009; Lewis *et al.,* 2000) even found that classifying multispectral data like Landsat TM could yield even better results in vegetation mapping than classifying hyperspectral data if the former had higher radiometric resolution and signal-to-noise ratio. They argued that relative differences across broad spectral bands can be more relevant than across multiple narrow bands.

---

[11] Landsat Headlines. Accessed on December 29, 2012: http://landsat.usgs.gov/
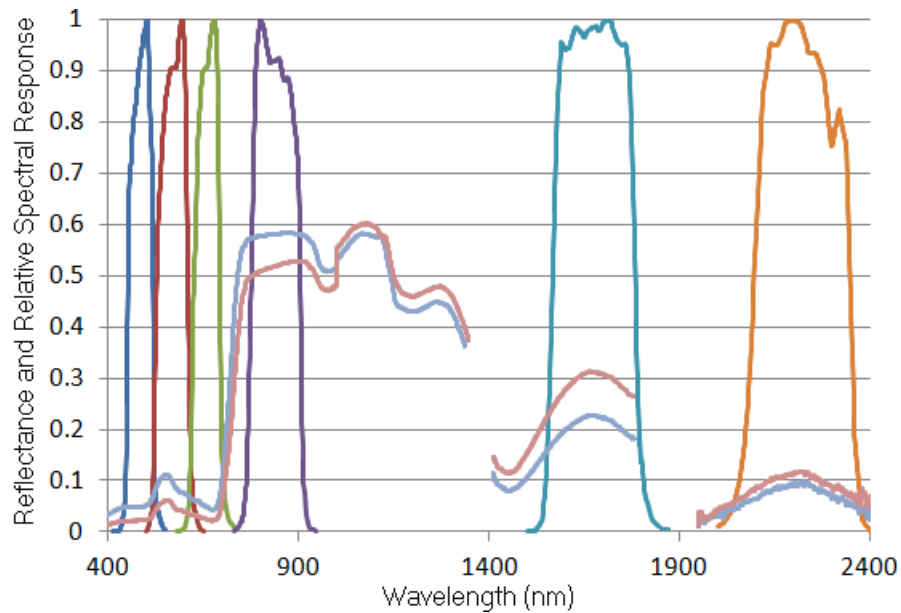
Figure 3.2: Landsat 5 TM relative spectral response curves shown with wheat and pea spectra.

Landsat imagery has been the most widely used data type for land-cover mapping due to its relatively high temporal and spatial resolution, as well as the long history of data acquisition (Haralick and Shanmugam, 1973; Knorn *et al.,* 2009). Since Landsat data became available for free in late 2008, the amount of downloaded scenes has increased to nine million[12] (as of September 1, 2012).

Hyperion is the first civilian hyperspectral imager operating in space and focused on terrestrial applications (Pearlman *et al.,* 2003). It employs an along-track push-broom sensor technology, using a 2-dimesional detector array that can capture an entire line of data across track simultaneously in all 242 spectral bands. This design requires no moving parts, which are prone to wearing out. It also provides increased dwell time, allowing for a higher spatial resolution and signal-to-noise ratio. Another major

---

[12] Landsat and LDCM Headlines 2012. Accessed on October 6, 2012:
http://landsat.usgs.gov/mission_headlines2012.php

31

advantage is the higher geometric fidelity. The disadvantages are a narrower field-of-view (i.e., narrower swath coverage) and various kinds of artifacts in the acquired imagery due to the sensor's complexity. A very complex optical system is used to project radiant energy onto the focal plane, and even thorough calibration does not guarantee proper wavelength representation of pixels in spectral bands, requiring sophisticated image preprocessing routines as discussed in the next section (Khurshid *et al.*, 2006).

3.4   Image Preprocessing

The proposed labeling technique requires accurate atmospheric correction because spectral characteristics of image clusters can be compared to reference spectra only when the brightness values are converted to surface reflectance by removing atmospheric scattering and gaseous effects.

Landsat 5 TM imagery is distributed in the form of Level 1 Terrain (1T) data product. 1T images are derived from Level 0 (raw) unprocessed images by converting pixel values into units of absolute radiance (32 bit) and scaling it to eight-bit calibrated digital numbers. The user must convert these numbers to at-sensor radiance using specific rescaling factors prior to atmospheric correction (Chander and Markham, 2003). Level 1T Landsat images are georeferenced to the UTM map projection, geometrically and radiometrically corrected[13].

Hyperion data are available from the USGS website as either Level 1Gst or Level 1R processed data. Level 1Gst images are terrain corrected and provided in 16-bit at-

---

[13] Landsat Processing Details. Accessed October 6, 2012:
http://landsat.usgs.gov/Landsat_Processing_Details.php

sensor radiance values, whereas 1R products are only radiometrically corrected[14]. A 1R image was used in this study because in 1Gst images the radiance is affected by pixel resampling. Geometric correction of the Hyperion data was not required since they were used only for the extraction of spectral signatures.

The preprocessing of the Landsat images was performed using the Landsat Calibration and FLAASH (Fast Line-of-sight Atmospheric Analysis of Spectral Hypercubes; Cooley *et al.,* 2002) modules of ENVI (the Environment for Visualizing Images; ITT Visual Information Solutions, Boulder, CO). The Landsat Calibration tool was used to convert uncalibrated digital numbers (DNs) to radiance in units of $\mu W/(m^{-2}$ sr^{-1} nm^{-1}). As FLAASH requires data to be in these units, the Band Math tool in ENVI was used to divide the resultant pixel values by 10. The FLAASH module was then applied to estimate at-surface reflectance from at-sensor radiance based on the selected atmospheric and aerosol models.

An atmospheric correction was carried out using the built-in MODTRAN (MODerate resolution atmospheric TRANsmission; Berk *et al.,* 1989) Radiative Transfer model in FLAASH. MODTRAN is the most widely used atmospheric model in remote sensing, which is embedded in several atmospheric correction procedures to estimate overall atmospheric transmission and scattering (Berk *et al.,* 1989). The model assumes that the atmosphere consists of horizontally homogeneous layers of certain gaseous and particulate composition[15]. Different gases and particles have different absorption and

---

[14] EO-1 (Earth Observing-1). Product Description. Accessed October 6, 2012:
http://eros.usgs.gov/#/Find_Data/Products_and_Data_Available/ALI
[15] About Modtran. Accessed October 6, 2012:
http://modtran5.com/about/index.html

scattering properties defining the atmospheric transmission. MODTRAN has several built-in atmospheric models (Sub-Arctic Summer, Mid-Latitude Winter, Tropical, etc.), each having a specific constituent profile for the atmospheric layers. Besides selecting the model, the user has to specify the latitude, longitude, aerosol type (e.g., rural, maritime, or urban), date and time of image acquisition, sensor altitude, pixel size, etc. Based on the estimated atmospheric transmittance and scattering coefficients, FLAASH derives approximate surface reflectance from at-sensor radiance.

Table 3.2 lists the parameter values selected for the atmospheric correction of the Landsat image data used in the study. Most of the values were obtained from the metadata file, while the value for the Initial Horizontal Visibility parameter was found on the Environment Canada website[16].

Table 3.2: Selected FLAASH parameters for the atmospheric correction of the Landsat TM image data.

Latitude	49°44'28.68"N	Ground Elevation	0.9 km
Longitude	112°32'45.93"W	Initial Visibility	48.3 km
Sensor Altitude	705 km	Atmospheric Model	Sub-Arctic Summer
Flight Date	2005-07-03	Aerosol Model	Rural
Flight Time GMT	18:05:23	Pixel Size	30 m

Unlike the correction of the Landsat data, the preprocessing of the Hyperion data required not only atmospheric correction, but also the removal of various spatial and spectral artifacts. Accurate prepossessing of the Hyperion data was implemented in the Imaging Spectrometer Data Analysis System (ISDAS; Staenz *et al.,* 1998), using a procedure described by Khurshid *et al.* (2006; Figure 3.3).

---

[16] National Climate Data and Information Archive. Accessed October 6, 2012: http://climate.weatheroffice.gc.ca

```
┌─────────────────────────────┐
│      At-Sensor Radiance      │
└─────────────────────────────┘
              ↓
┌─────────────────────────────┐
│  Spatial Shift Correction for the  │
│      Short-Wave Infrared      │
└─────────────────────────────┘
              ↓
┌─────────────────────────────┐
│          Destriping          │
└─────────────────────────────┘
              ↓
┌─────────────────────────────┐
│    Angular Shift Correction   │
└─────────────────────────────┘
              ↓
┌─────────────────────────────┐
│       Noise Reduction        │
└─────────────────────────────┘
              ↓
┌─────────────────────────────┐
│       Smile Detection        │
└─────────────────────────────┘
              ↓
┌─────────────────────────────┐
│    Atmospheric Correction     │
└─────────────────────────────┘
              ↓
┌─────────────────────────────┐
│       Smile Correction       │
└─────────────────────────────┘
              ↓
┌─────────────────────────────┐
│     At-Surface Reflectance    │
└─────────────────────────────┘
```
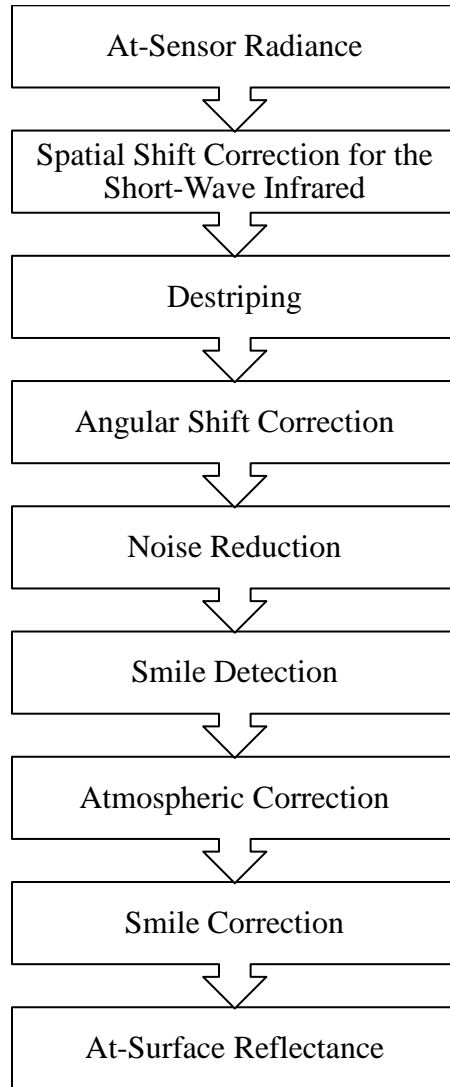
Figure 3.3: Preprocessing of the Hyperion data according to the procedure described in Khurshid et al. (2006).

The first three steps are used primarily to remove geometric artifacts. In the short-wave infrared bands, the right half of the image is shifted one pixel down in relation to the left side of the image (Khurshid *et al.,* 2006). This was corrected using the Spatial Shift tool in ISDAS. Secondly, the Auto-Destriping tool was used to correct vertical stripes. These stripes are columns of darker or brighter pixels that result from calibration differences in the detector array (Khurshid *et al.,* 2006). Principal Component Analysis can be used to reveal the severity of the striping problem as shown in Figure 3.4 (Staenz

and Williams, 1997). ISDAS fills the stripes based on the natural variations of adjacent pixels using spectral moment matching (Sun, *et al.,* 2005). Thirdly, there is an angular shift of 0.22° between the visible and near infrared (VNIR) and short-wave infrared (SWIR) data sets. This misalignment is due to the fact that the VNIR and SWIR data are recorded by two separate spectrographs resulting in data sets which are not perfectly co-registered. The Align Detector tool in ISDAS was applied to spatially align these data sets.
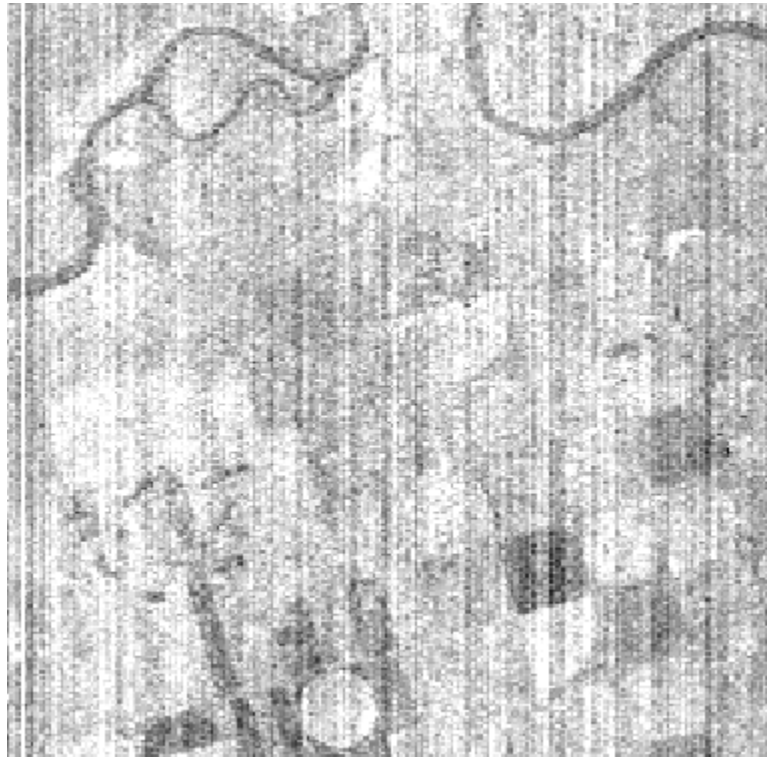
Figure 3.4: Principal Component 20 of the Hyperion image data before destriping. It contains a very small percentage of the data variance and is primarily an error band.

After performing destriping and geometric alignment, bands with low signal-to-noise ratio (SNR) were removed. A total of 44 out of the 242 spectral bands of Level 1 Hyperion images contain no useful information. All pixels in these bands have a value of zero. Specialists at TRW Inc. responsible for the calibration of Hyperion data chose not

to calibrate these bands due to insufficient signal at the extremes of the spectral range (bands 1 – 7 and 225 – 242) and in the overlapping region of the VNIR and SWIR bands (bands 58 – 76) (Barry, 2001). Following the ISDAS protocol (Khurshid *et al.,* 2006), bands 1-7, 221-242 and 56 – 76 were deleted from the data set, leaving 192 calibrated bands.

The ISDAS Average Smooth tool was used to remove the random noise and to increase SNR. This module creates a noise cube on a per-pixel basis using the digital-number-to-radiance gain coefficient frame provided with the Hyperion data and applies this noise cube to correct pixel spectra (Khurshid *et al.,* 2006).

The most important step of the preprocessing was the atmospheric correction of the data set. As in FLAASH, the central element of atmospheric correction in ISDAS is the MODTRAN radiative transfer model. The values specified for most of the parameters were the same as those specified for the correction of the Landsat data (Table 3.3). Pixel size and sensor altitude are the same for both sensors, while latitude, longitude, ground elevation, atmospheric and aerosol model are the same because both scenes cover the same area; the atmospheric conditions were also similar. Unlike Landsat 5 TM, Hyperion data contain bands covering the 940 nm and 1130 nm atmospheric water vapour absorption features, allowing the retrieval of water vapour. This parameter constitutes one of the dimensions in the resultant atmospheric correction look-up tables, which are required not only for the atmospheric correction, but also for the correction of the smile/frown effect (Staenz and Williams, 1997).

Table 3.3: Selected parameters for the atmospheric correction of the Hyperion data.

Latitude	49°44'28.68"N	**Ground Elevation**	0.9 km
Longitude	112°32'45.93"W	**Initial Visibility**	48.3 km
Sensor Altitude	705 km	**Atmospheric Model**	Sub-Arctic Summer
Flight Date	2005-07-02	**Aerosol Model**	Rural
Flight Time GMT	18:14:22	**Pixel Size**	30 m

The spectral line curvature (so-called smile/frown) effect is an artifact common for push-broom sensors (Herring *et al.,* 1993). This effect is characterized as an across-track wavelength shift (Jupp, 2001; Aktaruzzaman, 2008). If plotted as a function of pixel column number, this shift takes the form of a smile or frown (Figure 3.5). Due to this effect, the leftmost and rightmost pixels in a single band may have a slightly different band centre wavelengths than the pixels in the middle of the image. The smile/frown effect was detected before and removed after the actual atmospheric correction.

ENVI's EFFORT (the Empirical Flat Field Optimal Reflectance Transformation) polishing tool was applied on the resultant reflectance spectra to remove spikes. This tool minimizes the effect of systematic calibration and atmospheric correction errors using a parametric model based on Legendre polynomials (Boardman, 1998). After the polishing, the pixel spectra appear almost like ground-measured spectra, besides the noisy part above 2000 nm (Figure 3.6).
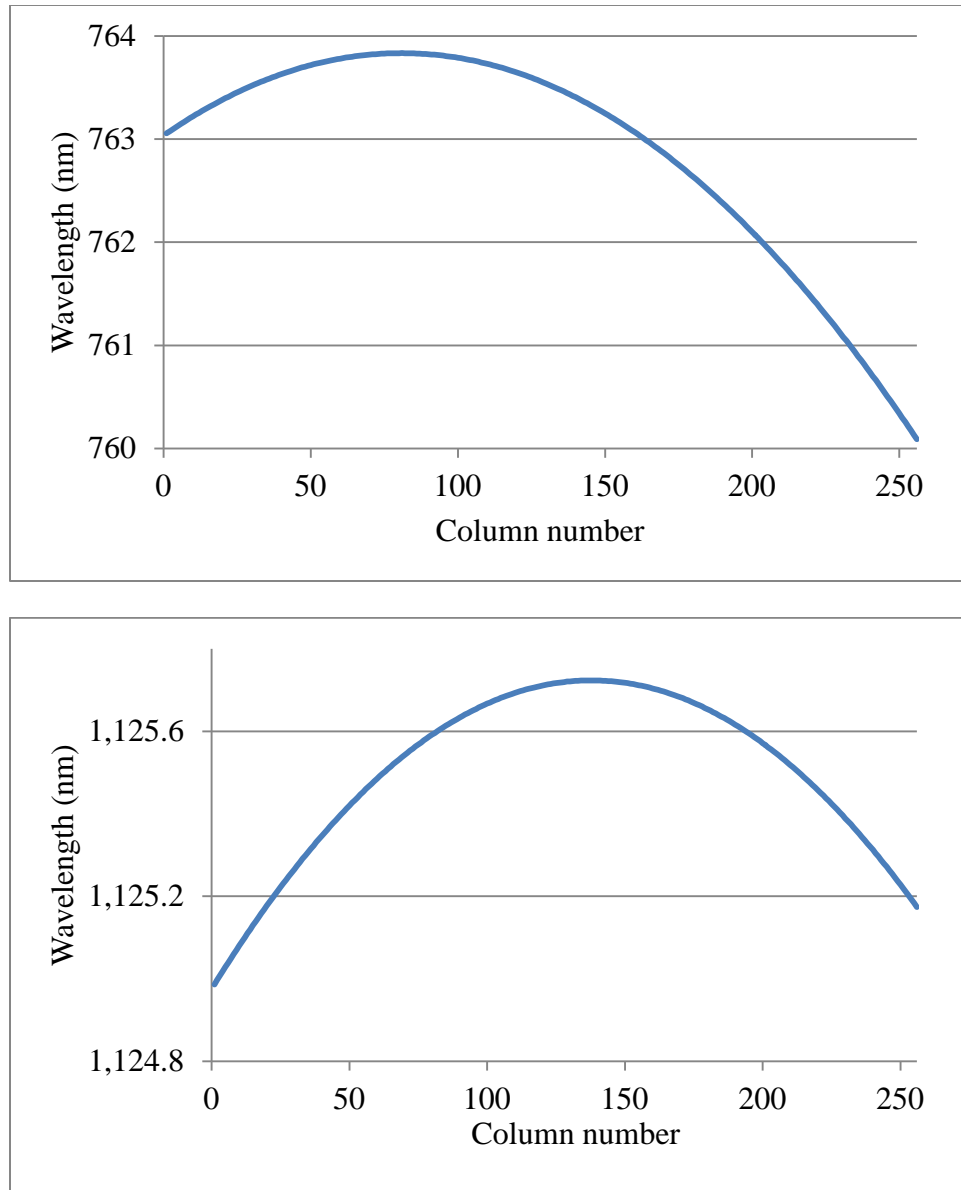
Figure 3.5: Frown curves for bands 41 (top) and 88 (bottom) of the Hyperion image. The plots illustrate the difference between the stated band centers for band 41 (762.6 nm) and 88 (1123.4 nm) and the actual wavelengths at which the signal was recorded.
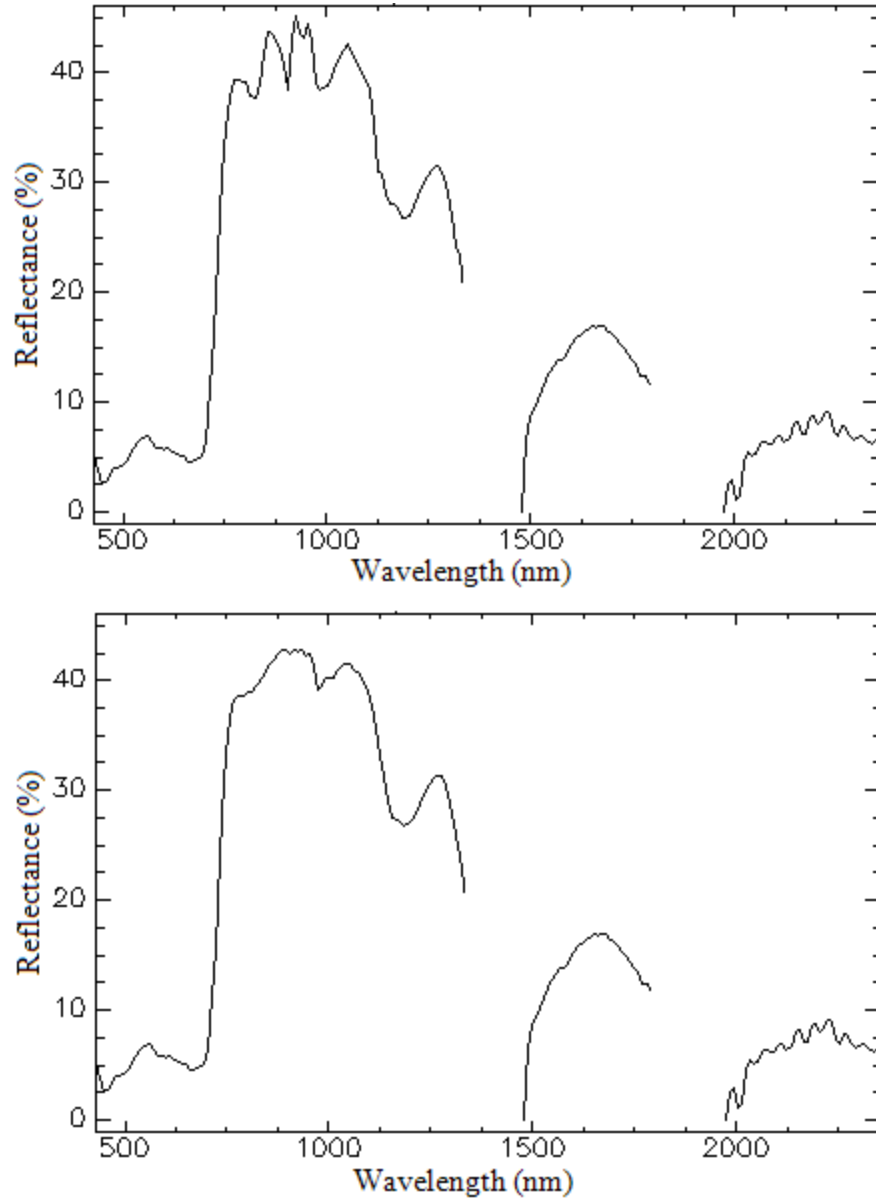
Figure 3.6: Pixel spectrum before (A) and after (B) EFFORT polishing. Plot C shows a ground-measured spectrum for comparison.

3.5   Acquisition of Spectral Signatures

Two approaches to signature extraction were tested. One approach was based on finding endmembers (pure pixels) using ENVI's Pixel Purity Index (PPI). According to this approach, if a pure pixel (i.e., a pixel with a high crop-to-soil ratio) is found in the same crop field with a ground reference point, its spectrum is saved as the spectral

signature of the crop type. However, for Hyperion data with their 30-m spatial resolution, crop fields are spatially homogeneous (i.e., contain pixels of similar purity). This presents a challenge to the PPI algorithm, causing it to find either too many or too few endmembers (Figure 3.7). Due to this reason, the PPI method was discarded as unsuitable for the specific application of this study.
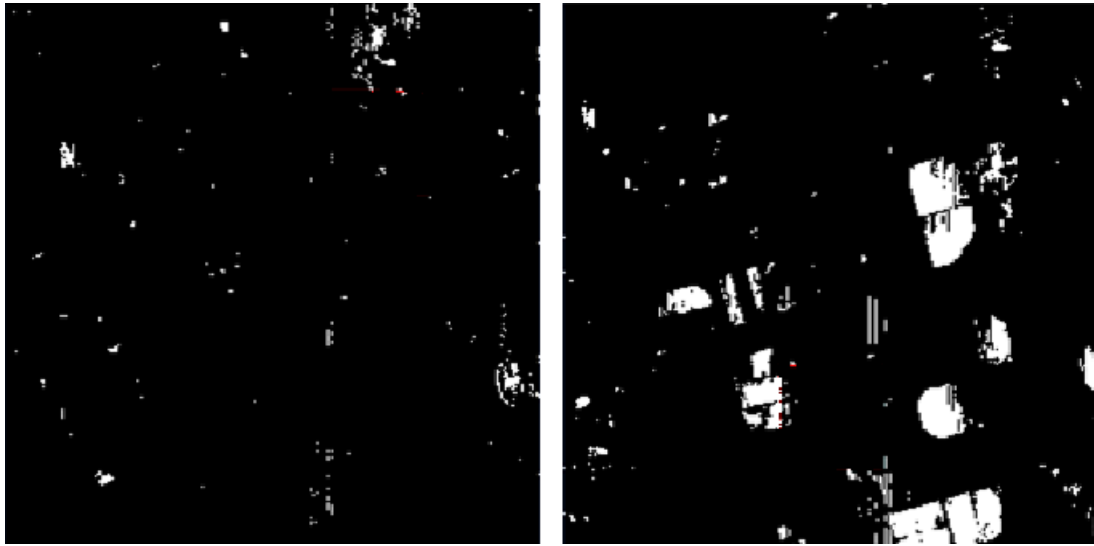
Figure 3.7: ENVI's Pixel Purity Index (PPI) algorithm finds either too few (left) or too many (right) pure pixels due to the homogeneity of crop fields at the spatial resolution of the Hyperion image. White pixels represent pure pixels.

Another approach involves the selection of regions of interest (ROI) in ENVI and using the mean reflectances in these regions as signatures. In this study, ROIs were delineated manually within fields of known crop type based on ground-reference data (Figure 3.8). Buffer zones of at least two pixels (approximately 60 meters) in width separated the edges of ROIs and the edges of crop fields to ensure the selection of pure pixels.

41
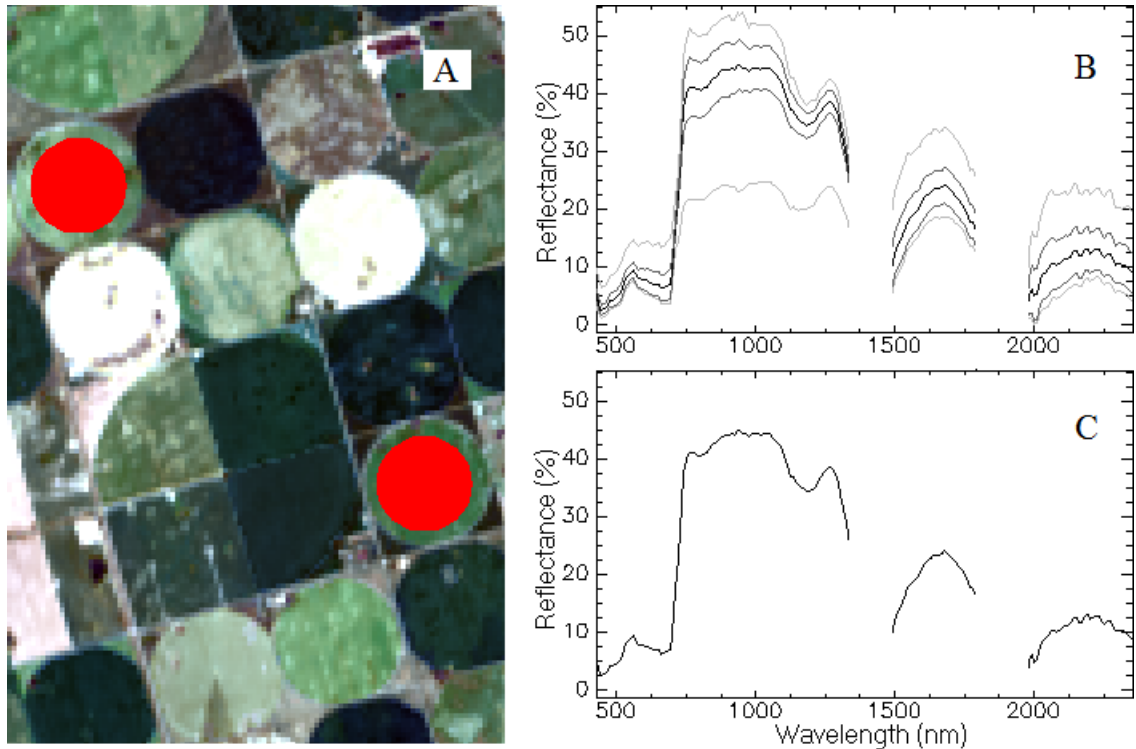
Figure 3.8: Spectral signatures of the crop types were obtained from the Hyperion image using the Mean-Reflectance-in-ROI approach. In this case, two regions of interests (ROIs; red circles) were selected in ground-referenced fields (A) and reflectance statistics (mean, min, max, and standard deviation) were extracted from these ROIs using ENVI 4.7 (B). The mean reflectance of the ROIs was used as the spectral signature as shown, for example, for potato (C).

To test how the labeling algorithm copes with different kinds of spectra, spectral signatures of water and dry grass were downloaded from the United States Geological Survey (USGS) website[17] and included in the spectral library. These spectral signatures were recorded using a spectrometer with a much higher spectral resolution than that of the spectral signatures retrieved from the Hyperion data.

---

[17] USGS Digital Spectral Library. Accessed October 6, 2012:
http://speclab.cr.usgs.gov/spectral.lib06/ds231/datatable.html

3.6   Spectral Separability of Crops

Spectral characteristics of crop fields in the Landsat image were compared with one another to find if fields of the same crop type were spectrally similar and whether different crops can be easily discriminated. This was accomplished in ENVI using the ROI Tool to select fields and the Compute ROI Separability tool to find the degree of separability. These values range from 0 to 2.0 and are computed using the Jeffries-Matusita and Transformed Divergence measures as described by Swain and Davis (1978). A value greater than 1.9 indicates that the ROI pair is statistically separable. Fields with higher separability were chosen for the extraction of spectral signatures and the selection of training areas.

3.7   Classification Method

The ISODATA clustering algorithm was chosen as it is one of the most widely used classifiers (Ball and Hall, 1965; Tou and Gonzalez, 1977; Xie *et al.,* 2008). In this study, two ISODATA-generated classified images were used: one with 20 clusters and one with 100 clusters. The labeling of the 100-class image could not be carried out manually due to insufficient ground-reference data. Therefore, the results from automatic labeling could be compared only to the results from manual labeling of the 20-class image.

3.8   Automatic Labeling

The approach to automation presented in the thesis is based on using a newly developed post-classification procedure that employs a spectral matching technique to

label classes generated by an unsupervised classifier. The procedure is designed to be quick and versatile.

The automatic class labeling program was written in the IDL programming language as an extension to ENVI. This made it compatible with remote sensing image and spectral library formats. The program can perform automatic labeling right after image classification within the ENVI environment. It can use images acquired by any multispectral sensor and provides the possibility to choose the spectral matching technique to be used. The program outputs two labeled classified images in the ENVI Classification image format. One image is a "soft" thematic map where the number of classes is the same as in the unlabelled image. Labels in this case indicate the three closest matches (e.g., "potato=3.28659; canola=3.80892; alfalfa=4.78866"[18], where potato is the closest match). The other image is a "hard" map in which classes with the same best match are merged (for example, classes "potato=3.28659; canola=3.80892; alfalfa=4.78866" and "potato=3.83582; flax=3.99791; canola=4.33457" are merged into one class "potato").

3.8.1   Spectral Resampling

Before performing spectral matching, the algorithm resamples the hyperspectral reference spectra to match the spectral characteristics of the image data to be classified. This was achieved using the relative spectral response profiles of the Landsat 5 TM bands (Figure 3.9). ENVI 4.7 includes relative spectral response data for 29 multispectral systems. This means that images acquired by any of these sensors can serve as input.

---

[18] In this case, numbers represent the Z-Score Distance (Section 3.8.3).
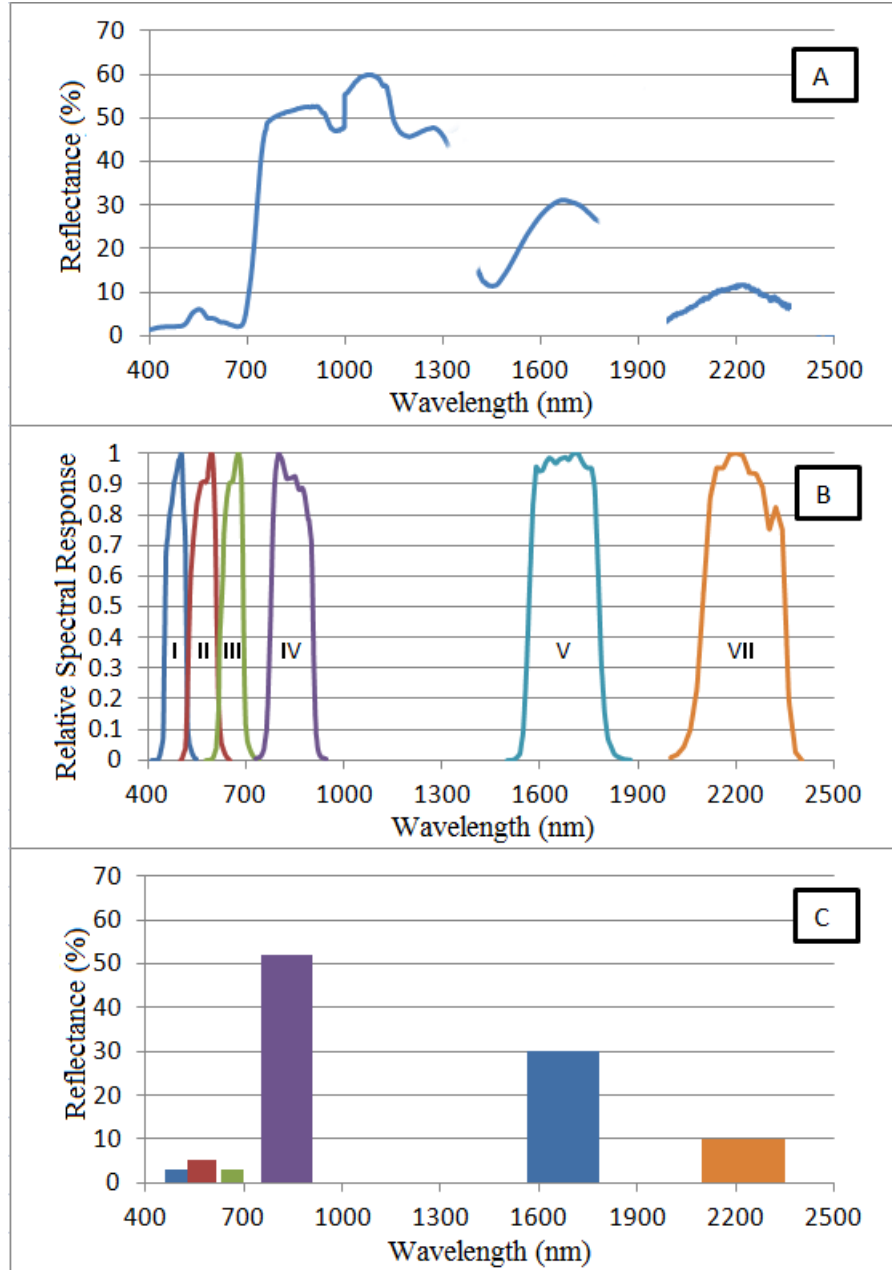
Figure 3.9: An example of spectral resampling. A) Spectral signature of wheat acquired using an ASD spectroradiometer; B) Relative Spectral Response Curves for the Landsat 5 TM bands; and C) Resampled spectral signature at the Landsat 5 TM spectral resolution (bar width represents band width at full-width half-maximum).

3.8.2 Existing Spectral Matching Techniques Used for Auto-labeling

The proposed spectral similarity measure was compared to the Spectral Angle Mapper (SAM) and the Correlation Similarity Measure (CSM) techniques (Section 2.3).

SAM was chosen because it is probably the most commonly used spectral matching technique (2,770 results in Google Scholar) and available in most image processing software packages (Luc *et al.,* 2005). It has been successfully used to classify Landsat data by a number of authors (Nangendo *et al.,* 2007; Chen *et al.,* 2009; Anggraeni and Lin, 2011) and was expected to provide good classification results. CSM was used as an additional method.

3.8.3 Z-Score Distance

SAM and CSM are designed to label individual pixels rather than clusters of pixels as they can only compare individual spectra. A new spectral matching technique was developed to address this issue. The technique was named *Z-Score Distance* (ZSD) due to the use of the z-score (standard score) statistical concept. The ability of ZSD to take into account the variation of pixel spectra within classes provides a major advantage over existing spectral matching techniques. While SAM and CSM could utilize only one parameter (mean class reflectance) in this study, the proposed technique used two - the mean and standard deviation[19].

The z-score is the number of standard deviations a datum (e.g., spectral signature) is away from the population or sample (e.g., spectral class) mean. The calculation of ZSD is similar to the Euclidean Distance (ED) calculation, but rather than the absolute distance, the relative distance is calculated based on the number of standard deviations of the class the reference spectrum is away from the class mean. This normalizes the amplitude of the differences in different bands, which is important as vegetation spectra

---

[19] Here, standard deviation refers to the deviation of pixel values for a particular spectral band in a particular class and not to the deviation of reflectance values among spectral bands within one spectrum as in the CSM equation (Equation 3.2).

vary at some wavelengths more than at others. For instance, Figure 3.10 shows that the variation of reflectance in Landsat TM band 4 (near infrared) is much greater than in the visible bands 1 – 3. The ZSD approach takes within-class variability as the baseline and calculates how much the difference between the reference spectrum and the class mean is greater or lower than this variation (standard deviation of the class). Perfectly matching spectra have a ZSD of 0; closely matching spectra would have a ZSD of less than 1. ZSD is calculated as follows:

$$\text{ZSD} = \sqrt{\sum_{b=1}^{n} \left((r_b - t_b)/\sigma_{t_b} \right)^2} \, , \qquad\qquad [3.3]$$

where **n** is the number of bands; r_b is the reflectance amplitude of the resampled reference spectrum in band **b**; t_b is the mean reflectance amplitude of the class in band **b**; σ_{t_b} is the class standard deviation in band **b**. For instance, in Figure 3.10, the reflectance amplitude in Landsat 5 TM band 1 of the resampled reference spectrum is 1.2 σ away from the class mean reflectance in the same band. The z-scores for the other 5 bands are 0.8σ, 1.9σ, -0.5σ, -2.1σ, and 1.1σ, respectively. With these values, the ZSD can be calculated as follows:

$$\text{ZSD} = \sqrt{1.2^2 + 0.8^2 + 1.9^2 + (-0.5)^2 + (-2.1)^2 + 1.1^2} = 3.4 \, . \qquad [3.4]$$

This distance is then compared with distances for other spectral signatures. The class is labeled with the name of the signature that has the smallest ZSD from the class mean in terms of reflectance.
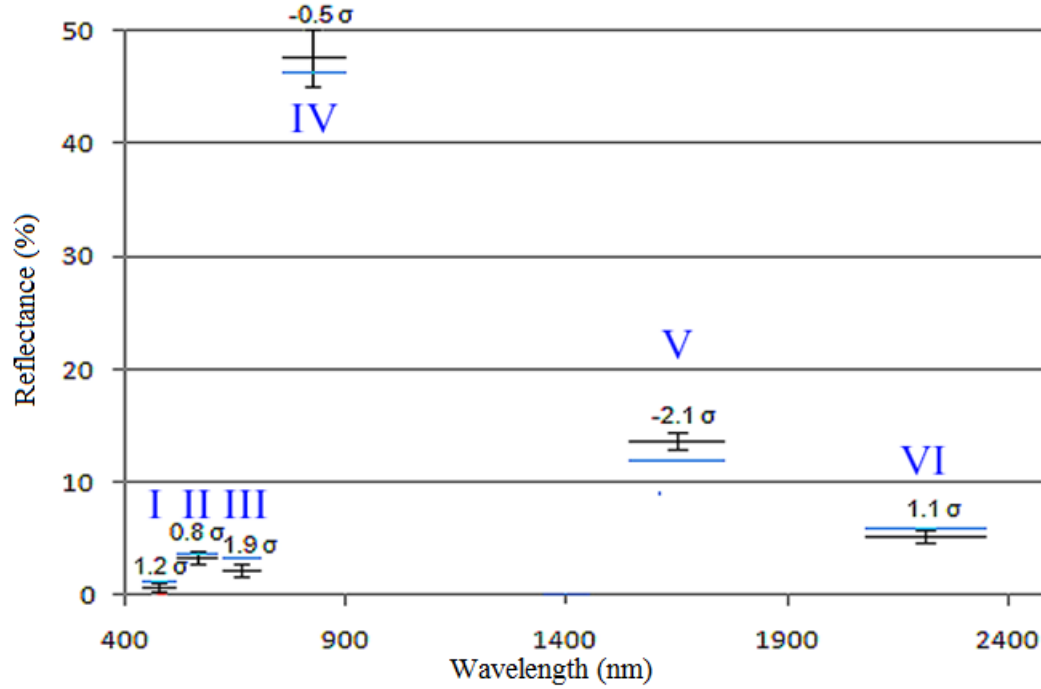
Figure 3.10: Resampled spectral signature (blue) and class mean and standard deviation (black). The reflectance amplitudes in the six Landsat 5 TM reflective bands (1 – 5 and 7) are compared. For example, the z-score for band 4 is smaller than for band 3, indicating a better match. The z-scores for all 6 bands are used to compute ZSD.

3.9   Classification Accuracy Measures

The overall accuracy, the Kappa coefficient, and the producer accuracy were used to assess the performance of the new technique and to compare it with existing classification methods. The overall accuracy shows the percentage of ground-referenced pixels that were classified correctly. The producer accuracy is the portion of classified pixels that matches ground-reference data for a particular class. The Kappa coefficient is used to find out if the accuracy level is significantly better than a random result, providing a better comparison of different classifications (Cohen, 1960; Smits *et al.* 1999; Congalton, 2001). These three measures are the most commonly used means of communicating the accuracy of classification results (Foody, 2008; Mitchell and Glenn, 2009; Huth *et al.*, 2012).

All accuracy measures can be derived from an error, or contingency matrix. An error matrix is a table in which columns show the number of ground-referenced pixels labelled as one land-cover type or another, while rows show the numbers for labelled pixels. For example, the numbers in Table 3.4 indicate that out of 1175 pixels ground referenced as canola only 605 were labelled correctly, meaning that the producer accuracy for this class is 51%. The overall accuracy is the sum of values in the main diagonal divided by the total number of ground-reference pixels (i.e., the sum of all values in the table). In this case, the overall accuracy is (31 + 1201 + 33 + 605 + 241 + 205) / (418 + 1201 + 35 + 1175 + 693 + 293) = 61%. The Kappa coefficient is (0.61 – 0.27) / (1 – 0.27) = 0.46, where 0.61 is the overall accuracy and 0.27 is the overall probability of chance agreement (i.e., correct classification by chance). One can say that the Kappa coefficient is the actual agreement minus the chance agreement. The calculation of the Kappa coefficient is described in detail in Congalton and Green (1991).

Table 3.4: An error matrix for five classes with rows representing classified data (predicted classes) and columns representing reference data (actual classes).

Class	Alfalfa	Barley	Beans	Canola	Potato	Sugar Beet	Total
Alfalfa	**31**	0	0	0	210	1	**242**
Barley	387	**1201**	0	340	0	0	**1928**
Beans	0	0	**33**	12	0	10	**55**
Canola	0	0	0	**605**	242	64	**911**
Potato	0	0	0	193	**241**	13	**447**
Sugar Beet	0	0	2	25	0	**205**	**232**
Total	**418**	**1201**	**35**	**1175**	**693**	**293**	**3815**

3.10 Accuracy and Performance Assessment

The provided ground-reference data contained 53 locations (GPS coordinates). Each point was located in a crop field, indicating what crop type was growing in the field. Only 33 ground-referenced fields were used for accuracy assessment as some fields were used for the extraction of spectral signatures and training the Maximum Likelihood classifier with which the new technique was compared. An ROI was selected inside each ground-referenced field. Accuracy assessment was performed automatically in ENVI using these ROIs. The accuracy assessment algorithm of ENVI generated error matrices and calculated per-class and overall accuracy statistics.

It was determined which of the three spectral similarity measures, SAM, CSM, and ZSD, was most suitable for automatic class labeling. The accuracy of the map generated by the automatic labeling algorithm employing the best spectral matching technique was compared to the accuracy of maps produced using ENVI's automatic SAM classifier and semi-automatic Maximum Likelihood classifier.

3.11 Consistency of Classification

There are two indicators of consistency for classification methods (Cihlar *et al.*, 1998). One indicator is the similarity of results obtained by different analysts using the same data. Accordingly, several graduate students in the Alberta Terrestrial Imaging Centre of the University of Lethbridge were asked to perform Maximum Likelihood and ISODATA classifications to estimate the consistency of the classification methods using this indicator.

The other indicator is the similarity of results produced by one analyst classifying different sets of data. This indicator is more important for assessing the consistency of automated classification methods, especially those relying on the spectral characteristics of land-cover types. The spectral properties of land-cover types may change with distance and in time, affecting the classification accuracy (Cihlar *et al.,* 1998). Unfortunately, this indicator could not be used in this study due to the lack of data.

4   RESULTS

4.1   Image Preprocessing

After image preprocessing, the Hyperion and Landsat data were compared to ensure that the accuracy of the produced maps was not affected by the spectral accuracy of the reflectance images. The Hyperion data was corrected in ISDAS and FLAASH, and the two resultant reflectance images were resampled to the Landsat 5 TM resolution. Three ROIs were selected in the left, centre and right portion of the two resampled Hyperion images and in the same crop fields in the Landsat image, each 388 pixels in size (Figure 4.1). The average reflectance of these ROIs was compared band by band (Table 4.1). This was done to account for the smile effect in the Hyperion image. It was found that the deviation of the ISDAS-corrected Hyperion data from the Landsat TM data was smaller and more consistent than that of the FLAASH-corrected data. Therefore, the ISDAS-corrected image data was selected for the extraction of spectral signatures.
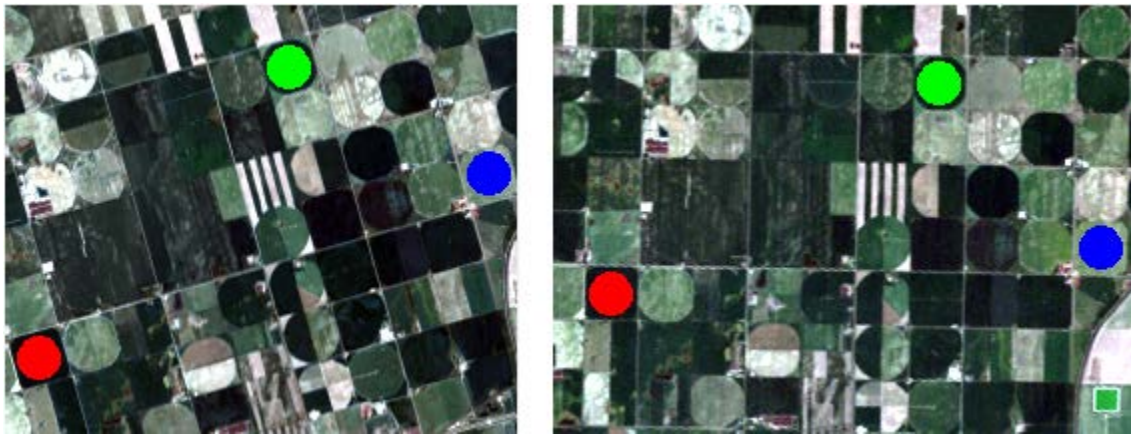
Figure 4.1: ROIs selected to compare the reflectance of the same crop fields in the ISDAS-corrected Hyperion data sets (left) and in the Landsat image (right).

Table 4.1: The Hyperion image was preprocessed in ENVI and ISDAS and the resultant images were resampled and compared to the atmospherically corrected Landsat 5 TM image. The mean reflectances of ROIs in the left, middle and right portions of the Hyperion image were compared. The difference in reflectance is enclosed in brackets.

Portion of image	Image	Reflectance (in %) for Landsat 5 TM Bands (Hyperion data were spectrally resampled to match Landsat 5 TM)						Avg. dif. from TM 5
		1	2	3	4	5	7	
Left	TM	1.7	3.6	2.2	46.4	11.5	5.2	
	ISDAS	2.1 (0.4)	4.0 (0.4)	2.5 (0.3)	44.9 (1.5)	10.3 (1.2)	3.9 (1.3)	0.8
	FLAASH	0.0 (1.7)	3.0 (0.6)	0.9 (1.3)	47.1 (0.7)	11.5 (0.1)	4.4 (0.8)	0.9
Centre	TM	1.8	4.0	2.3	53.2	15.7	6.8	
	ISDAS	2.4 (0.6)	4.6 (0.6)	2.9 (0.6)	52.4 (0.9)	14.6 (1.2)	5.6 (1.2)	0.8
	FLAASH	0.0 (1.7)	3.8 (0.2)	1.1 (1.2)	56 (2.8)	16.5 (0.8)	6.7 (0.2)	1.2
Right	TM	5.4	10.5	10.1	37.8	25.0	15.5	
	ISDAS	5.6 (0.2)	10.0 (0.5)	9.8 (0.3)	36.3 (1.5)	24.1 (0.9)	15 (0.5)	0.7
	FLAASH	4.3 (1.1)	10.7 (0.2)	9.8 (0.3)	36.2 (1.6)	26.6 (1.6)	16.5 (1.0)	1.0

The ISDAS-corrected image was expected to have higher spectral accuracy not only due to the smile correction, but also noise reduction and destriping. Many bands of the Hyperion image had noticeable noise and vertical stripes. These effects were successfully reduced in ISDAS using the Average Smooth and Auto Destriper modules (Figure 4.2). If not removed, the noise and stripes could affect the reflectance of the crop fields from which the spectral signatures were extracted (Section 3.4).
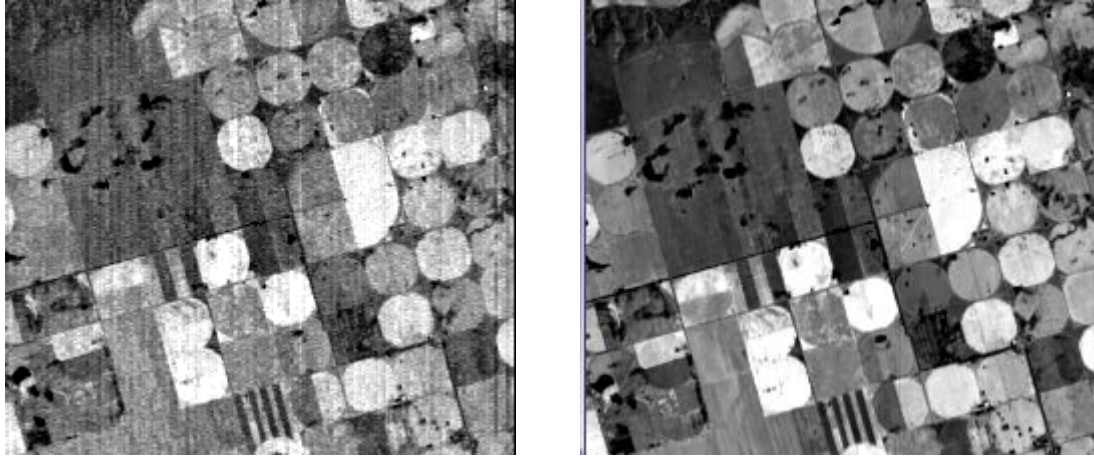
Figure 4.2: Band 77 (912.45 nm) of the Hyperion image preprocessed in ENVI (left) and ISDAS (right). In the right side image, stripes and noise were removed using the Auto Destriper and Average Smooth modules in ISDAS.

The visual examination of pixel spectra revealed that the reflectance curves in the infrared contain much more noise in the FLAASH- than in the ISDAS-corrected Hyperion data (Figure 4.3). In the FLAASH image, pixels representing vegetation had near-zero and even negative reflectance values in the blue region of the spectrum. On the other hand, pixel spectra in the ISDAS image had two abnormal drops in the near-infrared region. These abnormalities were successfully removed using the EFFORT module in ENVI, producing satisfactorily looking spectra (Figure 4.3 D).
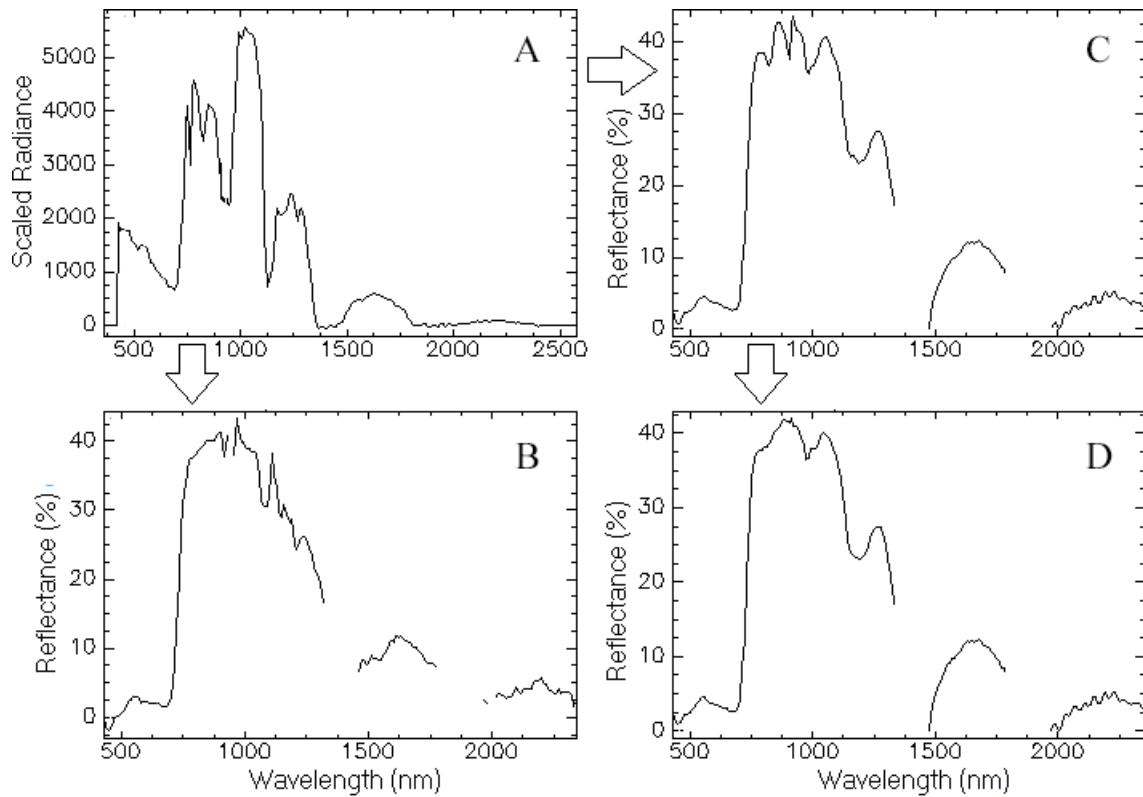
Figure 4.3: The spectrum of a pixel in the raw Hyperion image (A), corrected in FLAASH (B), ISDAS (C), and ISDAS + EFFORT (D).

4.2   Extracted Spectral Signatures

Thirteen spectral signatures were used in the study. Two signatures (water and golden dry grass) were downloaded from the USGS website[20], while the rest were extracted from the Hyperion image using the Mean-Reflectance-in-ROI approach (Section 3.5). The USGS signatures are essentially continuous with over 2000 bands, whereas the Hyperion signatures had 192 discrete spectral bands. The resampling part of the labeling algorithm handled both types of signatures equally well, providing the same result as ENVI's spectral resampling tool.

---

[20] USGS Digital Spectral Library. Accessed October 6, 2012:
http://speclab.cr.usgs.gov/spectral.lib06/ds231/datatable.html

In nearly half of the cases, the spectra of barley, grass and wheat fields were not statistically separable (Jeffries-Matusita distance less than 1.9; Figure 4.4). Grasses and cereals in particular are spectrally very similar during the mid-summer period, before the heading stage (Draeger *et al.*, 1971), resulting in poor differentiation leading to potential misclassification. Not only high spectral similarity among classes, but also high spectral variability within classes was observed. At the same time, high within-class variability was observed. For example, some barley, canola, and wheat fields were spectrally very different from other fields of the same crop type (Jeffries-Matusita distance greater than 1.9). For the two flax fields in the study area the Jeffries-Matusita distance was equal to 2.0, which is the maximum value for this index, indicating the fields are in no way similar. Due to this reason, both training and accuracy assessment ROIs were selected in different parts of the same flax field.
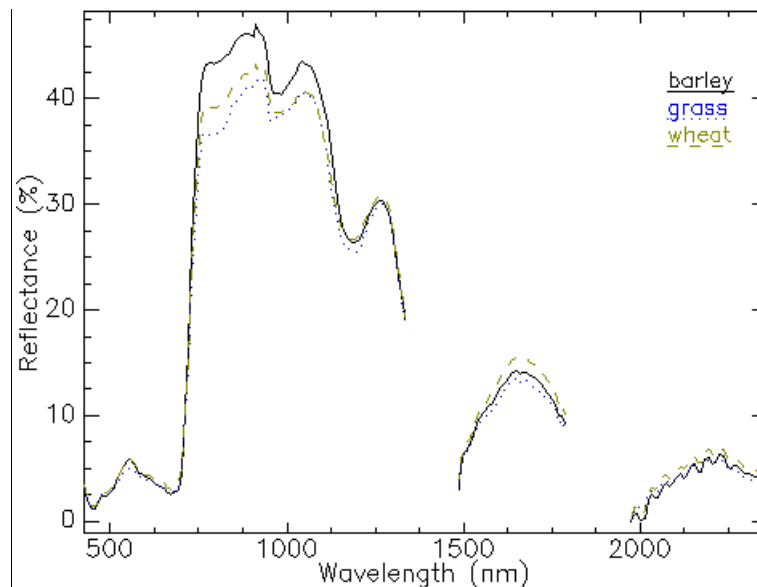
Figure 4.4: Barley, grass and wheat spectra extracted from the Hyperion image.

Among other factors, high spectral variability within classes could be caused by differences in canopy water content. The water band index (the reflectance at 900 nm divided by the reflectance at 970 nm), which was suggested by several authors as a good indicator of plant water content (Penuelas *et al.*, 1993; Gamon *et al.*, 1999), varied greatly among individual fields of the same crop type. For instance, the index ranged from 0.98 to 1.11 among individual canola fields.

Figure 4.5 shows the spectral signatures for the eleven crop types of interest. Although all thirteen spectral signatures were used for labeling, classification accuracy was assessed only for the eleven agricultural classes but not for the water and dry-grass classes.
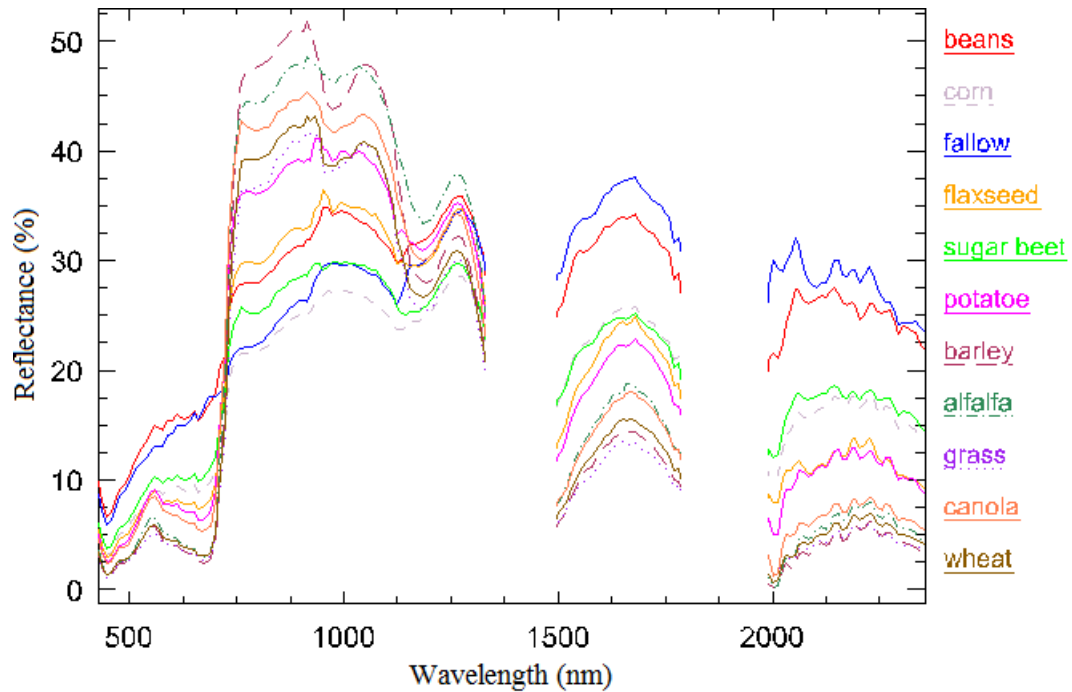
Figure 4.5: Spectral signatures of the crop types to be classified. These crops have very similar spectra, making it difficult to classify them in remote sensing images.

4.3   Accuracy Assessment Results

The accuracy and performance of the applied classification methods were assessed through several steps using error matrices generated automatically in ENVI (Tables 4.2 – 4.7). First of all, the accuracy of automatic labeling of the 20-class image was compared with that of manual labeling. The automatic labeling of the 20-class image was then compared with the automatic labeling of the 100-class image after the merging of classes of the same crop type. In addition, a number of spectral matching techniques (ZSD, SAM, and CSM) were compared to assess which provided better classification results when used for class labeling. Finally, the accuracy of the classified image labelled by the best spectral matching technique was compared with the accuracy of maps produced using three conventional classification methods: ISODATA with manual class labeling, SAM, and Maximum Likelihood. The effect of the spectral similarity of wheat, barley and grass on classification accuracy was evaluated.

The automatic labeling of the 20-class image using the ZSD technique was slightly more accurate (an overall accuracy of 47% with a Kappa coefficient κ of 0.41) than the manual labeling of the same image (average accuracy 43% among 5 analysts with the average κ = 0.36 as shown in Table 4.2). ZSD seemed to misclassify beans as fallow, canola as potato or flax, and corn as sugar beet (hereinafter referred to as "beet" in error matrices) or flax (Table 4.3). Both the SAM and CSM spectral matching techniques could not identify wheat and canola classes, which caused the accuracy to drop below the 30-% level (results not shown).

Table 4.2: Per-class producer accuracies (in %) for the maps produced by five analysts labeling the 20-class ISODATA image.

Class	Analyst 1	Analyst 2	Analyst 3	Analyst 4	Analyst 5	Average ± St. Dev.	Auto
Alfalfa	75.0	72.8	0.2	75.0	12.7	47.1 ± 33.5	74.82
Barley	48.0	53.9	49.5	48.0	49.5	49.8 ± 2.2	48.04
Beans	73.8	5.3	62.9	55.5	62.9	52.1 ± 24.1	7.42
Canola	25.5	11.8	9.9	9.9	21.9	15.8 ± 6.6	9.85
Corn	47.9	28.1	32.4	37.6	1.8	29.6 ± 15.4	30.08
Fallow	98.4	99.3	41.6	41.6	41.6	64.5 ± 28.0	99.34
Flax	77.1	62.9	87.3	72.2	70.2	74.0 ± 8.1	78.49
Grass	49.7	50.1	49.7	49.7	49.7	49.8 ± 0.2	49.74
Potato	55.4	61.1	54.6	60.0	54.6	57.1 ± 2.8	60.42
Beet	4.5	25.7	44.3	44.3	41.7	32.1 ± 15.4	38.34
Wheat	29.5	47.6	55.1	30.8	50.3	42.7 ± 10.5	49.31
Overall	44.5	45.5	42.3	41.8	40.1	42.9 ± 1.9	46.6
Kappa	**0.38**	**0.40**	**0.35**	**0.38**	**0.34**	**0.36 ± 0.02**	0.41

Table 4.3: Error matrix for the map produced using the proposed ZSD technique. ISODATA was set to generate 20 classes. The overall accuracy is 47% with the Kappa coefficient of 0.41. Numbers represent pixel counts.

Class	Alfalfa	Barley	Beans	Canola	Corn	Fallow	Flax	Grass	Potato	Beet	Wheat	Total
Alfalfa	**407**	595	0	334	0	0	0	0	68	0	302	1706
Barley	69	**577**	0	42	0	0	0	66	0	0	423	1177
Beans	0	0	**21**	0	24	0	0	0	0	7	0	52
Canola	0	0	0	**147**	1	0	0	0	208	1	6	363
Corn	0	0	0	88	**213**	1	22	0	0	149	0	473
Fallow	0	0	190	0	3	**599**	0	0	0	0	0	792
Flax	0	0	0	343	148	0	**405**	0	20	108	2	1026
Grass	0	0	0	0	0	0	1	**387**	0	0	66	454
Potato	0	0	0	493	60	0	85	0	**455**	76	5	1174
Beet	0	0	72	44	259	3	0	0	0	**212**	0	590
Wheat	68	29	0	1	0	0	3	325	2	0	**782**	1210
Total	**544**	**1201**	**283**	**1492**	**708**	**603**	**516**	**778**	**753**	**553**	**1586**	**9017**

As expected, the automatic labeling of the 100-class image produced better results than the labeling (both manual and automatic) of the 20-class image (Table 4.4). ZSD performed better than the other two spectral matching methods, yielding an overall accuracy of 51% (κ = 0.46) against 41% (κ = 0.34) and 33% (κ = 0.26) for SAM and CSM, respectively. SAM and CSM could not distinguish barley, grass and wheat. SAM labelled wheat and grass classes mostly as barley, while CSM misclassified barley and grass as wheat. SAM and CSM confused beans with fallow, whereas ZSD labelled them relatively well. ZSD was also better at identifying alfalfa and sugar beet.

Table 4.4: Error matrices for the maps produced using the 100-class image and Automatic Class Labeling technique employing three different spectral similarity measures: A) ZSD (overall accuracy is 51% and Kappa coefficient is 0.46), B) SAM (41%, 0.34) and C) CSM (33%, 0.26). Numbers represent pixel counts.

A Class	Alfalfa	Barley	Beans	Canola	Corn	Fallow	Flax	Grass	Potato	Beet	Wheat	Total
Alfalfa	**469**	340	0	94	1	0	0	13	3	1	377	1298
Barley	6	**795**	0	0	0	0	0	308	0	0	536	1645
Beans	0	0	**196**	21	47	29	0	0	17	16	0	326
Canola	13	65	0	**471**	14	0	34	24	124	23	55	823
Corn	0	0	0	60	**416**	0	2	0	1	69	0	548
Fallow	0	0	49	0	0	**572**	0	0	0	0	0	621
Flax	0	0	0	396	112	0	**307**	0	277	140	1	1233
Grass	0	0	0	0	0	0	1	**433**	0	0	183	617
Potato	0	0	0	446	97	0	218	0	**337**	55	63	1216
Beet	0	0	38	32	25	2	0	0	0	**257**	0	354
Wheat	56	1	0	0	0	0	0	0	0	0	**401**	458
Total	544	1201	283	1520	712	603	562	778	759	561	1616	9139

Table 4.4 (continued)

B Class	Alfalfa	Barley	Beans	Canola	Corn	Fallow	Flax	Grass	Potato	Beet	Wheat	Total
Alfalfa	**109**	1	0	50	1	0	1	433	119	1	588	1303
Barley	101	**1065**	0	35	0	0	0	234	2	0	666	2103
Beans	0	0	**22**	7	3	0	0	0	0	1	0	33
Canola	0	0	0	**757**	22	0	25	0	27	37	5	873
Corn	0	0	1	89	**397**	0	1	0	1	314	0	803
Fallow	0	0	259	0	15	**603**	1	0	0	20	0	898
Flax	0	0	0	346	191	0	**341**	0	301	177	0	1356
Grass	334	135	0	32	0	0	0	**87**	0	0	236	824
Potato	0	0	0	184	11	0	193	24	**309**	4	116	841
Beet	0	0	1	14	72	0	0	0	0	**7**	0	94
Wheat	0	0	0	6	0	0	0	0	0	0	**5**	11
Total	544	1201	283	1520	712	603	562	778	759	561	1616	9139

C Class	Alfalfa	Barley	Beans	Canola	Corn	Fallow	Flax	Grass	Potato	Beet	Wheat	Total
Alfalfa	**109**	1	0	111	0	0	1	361	119	0	209	911
Barley	0	**65**	0	5	0	0	0	0	0	0	0	70
Beans	0	0	**23**	7	37	0	0	0	0	1	0	68
Canola	0	0	0	**527**	16	0	25	0	5	12	1	586
Corn	0	0	1	64	**406**	0	31	0	0	161	0	663
Fallow	0	0	256	0	15	**414**	1	0	0	20	0	706
Flax	0	0	0	385	221	0	**414**	0	305	243	8	1576
Grass	1	861	0	8	0	0	0	**3**	0	0	485	1358
Potato	0	0	0	352	15	0	90	24	**328**	30	312	1151
Beet	0	0	0	1	2	0	0	0	0	**94**	0	97
Wheat	434	274	0	60	0	0	0	390	2	0	**601**	1761
Total	544	1201	280	1520	712	414	562	778	759	561	1616	**8947**

The overall accuracy was affected by the spectral similarity of wheat, barley, grass, and alfalfa. For example, when the class labeling in the 100-class image was

performed using the ZSD algorithm, wheat was classified correctly only in 25% while misclassified as barley or grass in 44% of cases. The figures for grass are 56% and 40%, respectively. If these three crops were treated as one class, the overall accuracy would rise from 51% to 62%.

Table 4.5 is the error matrix generated for the map produced using the SAM classifier. Surprisingly, SAM performed slightly better when it was used to label classes in the 100-class ISODATA image (41% overall accuracy, $\kappa = 0.34$) than when it was used as a stand-alone classifier to label individual pixels (39%, $\kappa = 0.32$). As a classifier, SAM was more successful only at identifying sugar beet. Whether it was used for labeling pixels or classes, SAM was unable to discriminate barley, wheat, grass and alfalfa.

Table 4.5: Error matrix for the map produced using the SAM classifier. The overall accuracy is 39% with $\kappa = 0.32$. Numbers represent pixel counts.

Class	Alfalfa	Barley	Beans	Canola	Corn	Fallow	Flax	Grass	Potato	Beet	Wheat	Total
Alfalfa	**31**	0	0	0	1	0	1	319	210	1	345	908
Barley	387	**1201**	0	340	0	0	0	389	0	0	1056	3373
Beans	0	0	**33**	12	12	1	0	0	0	10	0	68
Canola	0	0	0	**605**	56	0	129	0	242	64	5	1101
Corn	0	0	0	23	**334**	0	2	0	0	66	0	425
Fallow	0	0	248	0	6	**602**	1	0	0	0	0	857
Flax	0	0	0	304	249	0	**234**	0	52	202	0	1041
Grass	126	0	0	18	0	0	0	**39**	11	0	132	326
Potato	0	0	0	193	21	0	195	0	**241**	13	61	724
Beet	0	0	2	25	33	0	0	0	0	**205**	0	265
Wheat	0	0	0	0	0	0	0	31	3	0	**17**	51
Total	544	1201	283	1520	712	603	562	778	759	561	1616	9139

The accuracy of maps produced by five analysts using the Maximum Likelihood classifier ranged from 54% to 63% with an average of 58% (Table 4.6). The standard deviation of producer accuracies was greater than 10% for seven out of eleven crop types, indicating high inconsistency across most of the classes. As with the SAM classification, the common problem was the misclassification of grass and wheat as barley. Table 4.7 is the error matrix for the best Maximum Likelihood classification.

Table 4.6: Per-class producer accuracies (in %) for the maps produced by five analysts using the Maximum Likelihood classifier.

Class	Analyst 1	Analyst 2	Analyst 3	Analyst 4	Analyst 5	Average ± St. Dev.
Alfalfa	80.5	83.8	83.6	81.3	54.2	**76.7 ± 12.6**
Barley	71.9	79.0	73.1	68.7	77.1	**74.0 ± 4.1**
Beans	66.1	73.9	64.3	78.5	94.0	**75.3 ± 11.9**
Canola	68.4	61.3	57.8	75.7	77.4	**68.1 ± 8.6**
Corn	55.6	75.7	63.6	48.7	42.3	**57.2 ± 13.0**
Fallow	97.8	77.5	88.6	51.7	72.1	**77.5 ± 17.5**
Flax	98.9	97.0	99.3	97.0	97.2	**97.9 ± 1.1**
Grass	37.5	26.4	45.9	25.5	4.4	**27.9 ± 15.6**
Potato	97.4	91.8	80.5	67.5	64.7	**80.4 ±14.4**
Beet	23.0	41.4	40.5	21.2	24.4	**30.1 ± 10.0**
Wheat	30.0	24.7	10.6	26.1	22.3	**22.7 ± 7.3**
Overall & κ	62.5 (0.58)	61.6 (0.57)	58.0 (0.53)	53.2 (0.38)	55.7 (0.50)	**58.2 ± 3.9**

Table 4.7: Error matrix for the best Maximum Likelihood classification. The overall accuracy is 63% with κ = 0.58. Numbers represent pixel counts.

Class	Alfalfa	Barley	Beans	Canola	Corn	Fallow	Flax	Grass	Potato	Beet	Wheat	Total
Alfalfa	**438**	148	0	0	0	0	0	0	2	0	19	607
Barley	1	**864**	0	0	0	0	1	455	0	0	831	2152
Beans	0	0	**187**	32	14	8	1	0	0	117	0	359
Canola	4	108	0	**1040**	37	0	2	0	11	52	35	1289
Corn	0	0	50	33	**396**	3	1	0	0	29	0	512
Fallow	0	0	43	0	6	**590**	0	0	0	0	0	639
Flax	0	0	0	5	38	0	**556**	0	7	11	12	629
Grass	0	0	0	0	0	0	0	**292**	0	0	228	520
Potato	0	0	0	410	221	0	1	0	**739**	223	7	1601
Beet	0	0	3	0	0	2	0	0	0	**129**	0	134
Wheat	101	81	0	0	0	0	0	31	0	0	**484**	697
Total	**544**	**1201**	**283**	**1520**	**712**	**603**	**562**	**778**	**759**	**561**	**1616**	**9139**

4.4   Summary

This chapter presents the results of a technique developed to provide automated class labeling based on spectral similarity measures. Two existing spectral similarity measures, namely SAM and CSM, were tested, but neither of them provided satisfactory results (the overall accuracy of resultant maps was below 50%). ZSD, a new measure derived from the z-score statistical concept, could utilize more spectral information, providing maps of higher accuracy (51%) in comparison to maps produced by automatic class labeling using SAM and CSM, as well as manual class labeling (40% to 45% overall accuracy depending on the analyst). Maximum Likelihood classification provided better results than any other classification method tested, although the accuracy of resultant maps varied greatly from one analyst to another (from 54% to 63%).

No matter what technique was used, the major factor affecting the accuracy of resultant maps was the low inter-class and high intra-class spectral variability. High spectral similarity was observed among grasses (barley, wheat, and grass) and between canola and potato. Barley, canola, and wheat fields were also characterized by high within-class variability, causing individual crop fields of the same crop type to have different spectral properties.

Figure 4.6 compares all four classification methods tested. The automatic class labeling technique provided better results for alfalfa, beans, corn, grass and sugar beet, whereas canola, corn, fallow, flax, potato, and wheat were identified with similar or lower accuracy.
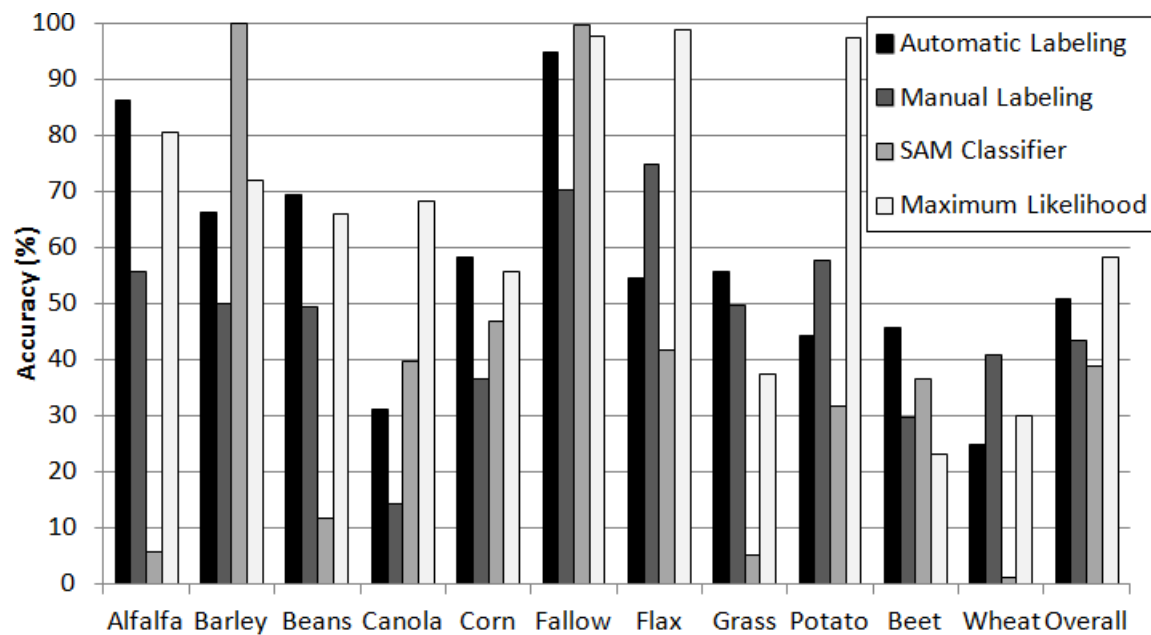

Figure 4.6: Per-class (producer) and overall accuracies for the maps produced using the four methods tested. The values for Maximum Likelihood and ISODATA with manual labeling are averaged values for five analysts.

5   DISCUSSION

5.1   Methodological Approach

The automatic class labeling technique described in the thesis differs from many other approaches to the automation of image classification in a number of ways. Some methods, like those based on reusing training areas, are not fully automated as they still require user intervention to classify at least one image in a series. The application of other techniques, such as decision tree algorithms, are limited or tuned to only one type of data. A few techniques are fully automated and can be used with images acquired by different sensors, but they need additional information about the study area, like in case of the Data Assisted Class Labeling technique.

The technique developed for this thesis follows an approach to automation that does not have the aforementioned disadvantages (Table 5.1). This approach is based on using a spectral matching technique to label pixels or classes based on the similarity of their spectra to reference spectra from a spectral library. This reliance on a spectral library with the simulation of any available satellite system as well as a robust statistical calculation of goodness of fit between the reference spectra and the classified pixel is the key development and contribution of this thesis. The only requirement is that the image to be classified and labeled requires an accurate atmospheric correction of the images prior to classification, as it assumes that pixel values are surface reflectance values. Hence, calculated reflectance values of the image must be as close to the actual surface reflectance of the scene as possible to generate a reasonable solution for the class label assignment. If reference spectra are not ground measured but extracted from

hyperspectral imagery, like in this study, the hyperspectral data must be accurately preprocessed as well.

Table 5.1: The advantages and disadvantages of different approaches to the automation of image classification as discussed in detail in Chapter 2.

Advantages (+) and Disadvantages (-)	Techniques					
	Decision Tree	Region Growing	Signature Extension	Training Area Reuse	Data Assisted Class Labeling	Spectral Matching
Full Automation (+)	+	+	−	−	+	+
Classification of Images from Different Sensors (+)	−	+	−	+	+	+
Need for Additional Data about the Study Area (−)	+	−	+	+	−	+
Need for Very Accurate Atmospheric Correction (−)	−	+	−	+	+	−

One of the disadvantages of the spectral matching approach is that the accuracy of resultant maps is dependent (among other factors) on the selection of spectral signatures. The classification of dynamic land-cover types, such as vegetation, requires very careful selection of spectral signatures. Seasonal physiological and structural changes effect the spectral characteristics of plants (Price, 1994). For this reason, the user must take into account the growth stages of plant species in the scene, especially if these species have distinct annual phenological cycles. Most agricultural crops are good examples of plants with explicit phenological stages (Section 1.5).

In this study, spectral signatures were extracted from a Hyperion data set that was acquired at the same time of day with just one day difference in relation to the Landsat 5 TM image collection. This means that crops in the two data sets were in the same phenological stage. In addition, both sensors have the same spatial resolution, meaning

the pixels in both data sets were equally mixed. Thus, the extracted spectral signatures actually represented mixed materials with the same ratio of the same constituents (soil and crop) as in the crop fields in the Landsat image. These two factors provided relatively high classification accuracy.

However, it is unlikely that the automatic labeling of classes in a different image using the same spectral signatures would yield high accuracy results because in that other image crops would have different spectral characteristics due to various factors, such as weather, irrigation practices, phenology, and variations in leaf coverage. Hence, the main drawback of the presented method, as well as any spectral matching classifier, is that it is based on using static spectral signatures to label very dynamic vegetation land-cover types.

Ideally, the user should have multiple pure (ground-measured) spectral signatures for various phenological stages, and the algorithm should be able to deal with the problem of mixed (soil and crop) classes. Perhaps, the algorithm could create mixed spectral signatures by combining crop spectral signatures with the soil spectrum at various area-cover ratios. However, having too many similar spectral signatures will make it harder for the algorithm to pick the right ones. The more spectral signatures are used, the lower classification accuracy should be expected. The user must use only the most relevant spectral signatures in order to achieve the best result.

A database like SPECCHIO can be used to find the most appropriate spectral signatures. This database has a descriptive metadata structure and allows querying spectra by date and time of acquisition, location, viewing angle, sensor, etc. It is possible to

develop an algorithm that retrieves spectra from such databases automatically using the metadata of the remote sensing imagery to be classified.

The automatic class labeling technique combines the spectral matching approach with unsupervised classification, inheriting the advantages and disadvantages of both. From the former it gets automation and dependency from the quality and selection of spectral signatures, while from the latter it takes the familiarity of conventional classification methods and the drawbacks of purely statistical grouping of pixels. In addition, the new technique has advantages and disadvantages of its own.

When used in conjunction with an unsupervised classifier, the class labeling algorithm faces the same problem as a human analyst does when they manually label spectral classes. Commonly used unsupervised classifiers (e.g., K-means or ISODATA) group pixels based solely on their spectral characteristics, ignoring the fact that many land-cover types (e.g., vegetation) have dynamic and multimodal spectral properties and a certain spatial pattern. For this reason, the accuracy of maps produced using unsupervised classification is never 100% due to the mismatch between the extent of spectral classes and the extent of actual land-cover types.

The mismatch between spectral classes and information-based classes could be reduced if crop fields were classified as objects rather than groups of spatially unrelated pixels. Object-oriented classification can produce maps that not only look better, but also have higher accuracy (Janssen and van Amsterdam; 1991; Manakos *et al.*, 2000; Aplin and Atkinson, 2004; Castillejo-González *et al.*, 2009). Simpler object-based methods involve using separate, manually created Geographic Information System (GIS) layers

69

(Janssen and van Amsterdam, 1991), while more complex approaches are based on image segmentation and other automated comprehensive image analysis techniques that use various spatial and spectral clues (Pal and Pal, 1993; Su *et al.*, 2008; Blaschke, 2010). A good example of the latter is the eCognition software[21], which can classify objects based on their shape, texture, size and relationship with other objects (Manakos *et al.*, 2000; Flanders *et al.*, 2003; Pakhale and Gupta, 2010). However, the fact that object-based classification techniques started to appear more than two decades ago and are still not commonly used indicates that they also have limitations with respect to classification accuracy.

The main challenge in the development of the class labeling algorithm was to find a suitable spectral similarity measure. Existing spectral matching techniques are used to compare individual spectra, while spectral classes are composed of multiple pixels with similar but not the same spectra. The study showed that existing similarity measures cannot be used to label classes because the accuracy of such labeling is unacceptably low. A new spectral matching technique named Z-Score Distance (ZSD) was developed to deal with this problem. It takes into account the variation of pixel spectra within classes, measuring the distance between the class spectra and reference spectra in units of the standard deviation. The testing of ZSD on the provided data set showed promising results.

ZSD provides the automatic class labeling method a number of advantages over commonly used semi-automated classification methods. When the number of classes is large, the use of existing classifiers (e.g., ISODATA and Maximum Likelihood) is

---

[21] eCognition software. Accessed on December 30, 2012: http://www.ecognition.com

impractical if no ground information is available. This is often the case for large countries

with a relatively small population size, such as Canada and Russia. Even when ground

reference data are available, it might be very scarce (and expensive) and should be used

entirely for accuracy assessment if the validation of classification results is required.

5.2   Results

A Landsat 5 TM image classified using the ISODATA unsupervised classifier and

crop spectral signatures extracted from a Hyperion data set were selected to test the

automatic class labeling algorithm. There are numerous examples of successful use of

this classifier and data acquired by these sensors for the classification of vegetation. The

extensive literature on the topic allowed a more comprehensive analysis of the results.

The first objective was to convert pixel digital numbers in the Landsat 5 TM and

Hyperion data sets into surface reflectance. The Landsat image was atmospherically

corrected using the FLAASH module in ENVI, while the Hyperion data was corrected

using FLAASH and the ISDAS software package. The resultant reflectance images could

not be validated because no relative ground-measured spectra were available. Therefore,

TM and Hyperion data were simply visually inspected for noticeable errors and compared

to one another. As the images were acquired at the same time of the day with just one day

difference, the reflectance of the same targets in the two images was expected to be

nearly identical.

The visual inspection of the atmospherically corrected Landsat image data did not

reveal any noticeable error. However, both FLAASH- and ISDAS-corrected Hyperion

data contained obvious systematic errors. Thus, the FLAASH-corrected image had very

71

low and sometimes even negative reflectances in the blue region of the electromagnetic spectrum. A probable cause is the overestimation of the path radiance, which is dependable on the aerosol optical depth (horizontal visibility) used. In addition, the reflectance spectra of pixels in the FLAASH-corrected data were very spiky in the region above 1000 nm. This can be explained mainly by the low signal-to-noise ratios of the Hyperion bands in this region.

The preprocessing in ISDAS included destriping and noise reduction steps, resulting in better looking spectra in the region above 1000 nm. On the other hand, there were two unexpected negative spikes in reflectance spectra at 820 nm and 905 nm, which could be caused by errors in the calibration of the data and underestimation of the water vapour. The EFFORT tool in ENVI was used to remove these spikes at these wavelengths, producing naturally looking spectra.

Both FLAASH- and ISDAS-corrected Hyperion reflectance data were resampled to the Landsat 5 TM spectral resolution and compared with the corrected Landsat image data. It was found that the FLAASH-corrected image data differed from the Landsat data more than the ISDAS-corrected ones. In case of the FLAASH-corrected data, the difference in the centre of the image was greater than the difference along its sides. This could indicate that the wavelength calibration algorithm of FLAASH was not able to properly correct the smile effect.

The developed post-classification technique labels spectral classes as thematic classes by matching the spectral characteristics of these classes with reference spectra. Any spectral matching algorithm can basically be used for this purpose. However,

existing algorithms are normally used to match individual spectra (i.e., the spectrum of a pixel to a reference spectrum) and are not well suited for class-labeling applications as they ignore intra-class spectral variability. A new spectral matching technique, the Z-Score Distance, was developed to address this issue. It uses not only the mean reflectance, but also the standard deviation of reflectance in the classes to be labelled. Among the three spectral matching techniques tested (Spectral Angle Mapper, Correlation Similarity Measure, and Z-Score Distance), the Z-Score Distance was the most suitable for the class-labeling application. It produced a map with an overall accuracy of 51%.

Automatic labeling provided better results in comparison to manual labeling (51% against 43% overall accuracy). It was not possible to manually label all classes in the 100-class ISODATA image due to the lack of ground-reference data. In fact, most of the classes would remain unlabelled (results not shown). For this reason, the results from automatic labeling of the 100-class image were compared with those from manual labeling of the 20-class image. The labeling of the 20-class image could not provide high accuracy results due to the pronounced mismatch between the distribution of spectral classes and the actual distribution of land-cover types in the scene.

The automatic class labeling technique outperformed the Spectral Angle Mapper classifier (51% against 39% accuracy). The specialty of this classifier (dealing with shadow effects) was not beneficial in this case as the study area was mostly flat with very little variation in illumination. On the other hand, the Maximum Likelihood classification generated better results (58% average overall accuracy among five analysts), although the accuracy varied greatly depending on the analyst's experience. This higher accuracy

might be explained by the fact that supervised classifiers assign pixels to one class or another not based on some arbitrary statistical rules, but rather based on similarity to the spectral characteristics of user-selected training areas, which are, by definition, representative patches of land-cover or land-use types.

The main advantage of the proposed procedure is that it is more consistent, faster, and easier to use than the Maximum Likelihood and other supervised classifiers. In comparison to the Maximum Likelihood and SAM techniques, automatic class labeling provided better results for alfalfa, beans, corn, grass, and sugar beet, whereas barley, canola, fallow, flax, potato and wheat were identified with similar or lower accuracy.

The results are in line with accuracies achieved using single-date data classification in agriculture (Ban, 2003; Eckert and Kneubühler, 2004; Blaes *et al.,* 2005; Leite *et al.,* 2008). Higher classification accuracy could be achieved if multi-temporal imagery was available (Section 1.5). The image data used in this study were acquired in early July when some crop types have nearly identical reflectance characteristics (e.g., wheat, barley and grass).

High within-class spectral variability was detected for some classes (barley, canola, flax, and wheat). This variability could be caused by a number of factors. First of all, the difference in reflectances among fields of the same crop type could have been caused by the variation in soil water content determined by weather and irrigation practices. Not all the fields in the scene were irrigated by central pivots, meaning that different fields could receive different amounts of water by different schedules. The water band index did indicate that plants in some crop fields could experience water

74

stress. Secondly, according to the reports by the Alberta Agriculture and Rural Development (AARD) for June 23, 2005, flooding in early June, hailstorms, leaf diseases, and fertilizer leaching damaged some crop fields in the area. Thirdly, crops in different fields were not seeded at exactly the same time and could be in different growth stages at the time of data acquisition. Lastly, all cultivars of the same crop were classified as one thematic class, although cultivars of the same crop type can have different spectral characteristics. Unfortunately, no information was available to support the last two statements.

6 CONCLUSIONS

The thesis describes a method that automates class labeling for unsupervised image classification. Rather than being another classifier, the proposed post-classification routine complements existing unsupervised classifiers, making them fully automatic, provided a hyperspectral library of spectral signatures exists.

Archives of remotely sensed data grow at an accelerating pace as more and more Earth observation satellites are being launched every year. Our ability to process image data cannot keep up with the rate of data acquisition due to the lack of automated procedures; a great portion of the data is stored in archives without being used for the generation of information products (e.g., maps). Fully automated image classification procedures could provide faster and more consistent generation of maps required for large mapping projects which are currently constrained by the need for expert analysts. The technique described in the thesis is the result of an attempt to create such a procedure.

Current image classification techniques rely on image analysts to label classes either before classification as used in supervised classification or *a posteriori* in unsupervised procedures. As a comparison, the new technique was evaluated against experts for both supervised and unsupervised classification.

The objective of the study was to develop an algorithm that can automatically label classes by matching their spectral characteristics to reference spectra. The objective was met: using a newly developed spectral matching technique and a library containing spectral signatures extracted from a Hyperion data set, the presented class labeling

76

procedure successfully labelled classes in a classified Landsat 5 TM image. The performance of the procedure was evaluated and compared with the performance of three commonly used image classification methods, namely ISODATA with manual labeling, SAM and Maximum Likelihood. For the data set used, the automatic class labeling algorithm did perform better than human analysts; however, it is yet to be determined if this remains true for other sets of data.

A new spectral matching technique named Z-Score Distance was developed specifically for the class-labeling application. It allowed the labeling algorithm to produce a map of higher accuracy than that of maps produced by any of the five analysts (51% overall accuracy against 43% average overall accuracy). The technique can generate maps of satisfactory accuracy if certain conditions are met; however, it cannot outperform reliable traditional supervised procedures like the Maximum Likelihood classification (58% average overall accuracy). In supervised classification, classes are user defined (i.e., the classifier "knows" what to look for), which improves the ability to differentiate among classes with similar spectral characteristics.

The consistency of class assignment is an important advantage of the presented technique. Class-assignment consistency guarantees that images acquired over similar areas (i.e., with the same vegetation types in the same growth states) can be classified with the same degree of accuracy, eliminating the need for accuracy assessment of every image in the series. This could be particularly useful for large scale projects where ground-reference data is limited in spatial extend. However, the assessment of the consistency of the developed automatic class labeling technique is the subject of future research.

The new technique can be used to label classes in images acquired by any multispectral and hyperspectral sensor and classified using any existing classifier. As new satellites are developed and corresponding spectral response data are added to the database, their bands can be computed by the spectral resampling algorithm and readily used by this technique. This renders the technique robust and flexible over time.

Given that the program was written as an extension to ENVI, all steps – image preprocessing, classification, class labeling and accuracy assessment – can be done automatically in ENVI, a software package commonly used by remote sensing specialists. The program can be integrated with other software packages as well.

The fast processing speed is a great advantage of the automatic labeling technique. Both selection of training areas in supervised classification and manual class labeling in unsupervised classification are very time consuming. In contrast, the new technique can label any number of classes in a fraction of a second.

The lack of vegetation reference spectra available in online spectral libraries is one of the main factors that prevent techniques based on spectral matching, such as the one presented, from being widely used for vegetation mapping. This will become less of an issue as more spectra are acquired and more private spectral libraries become available to the public.

Making a comprehensive library of vegetation spectra is a challenging task not only because of the large number of plant species, but also due to the fact that vegetation spectra are very dynamic. Such a library would have to contain multiple spectra for each plant species. For example, it should have spectra that characterize different phenological

stages and health conditions of each species. The current version of the HyspIRI Ecosystem Spectral Library[22] might be the first little step in this direction.

6.1   Future Work

The manual selection of spectral signatures from a large database for a specific application can be time consuming. An algorithm that automatically selects the most relevant spectral signatures could solve this problem. Together with the developed automatic class labeling technique, as well as any existing spectral matching classifier (e.g., the SAM classifier), this algorithm would make the whole processing chain of image classification fully automated.

Different decision rules for selecting the best match between a spectral class and reference spectra can be tasted. For example, when the spectral characteristics of a class match two spectral signatures almost equally well based on one spectral similarity measure (e.g., ZSD), the class-labeling program could use another measure (e.g., SAM) to verify the match. In addition, the program could provide information about the quality of the resultant match. When there are two or more close matches, the algorithm could assign the class to a broader category (e.g., cereals instead of barley or wheat) or at least notify the user about the possibility of an error.

It would be interesting to see how the technique performs with other targets and data types. Agricultural areas are among the most challenges surfaces on Earth to classify. It is likely that the class-labeling technique would generate maps of higher accuracy if used in the classification of land-cover types that have lower intra- and higher

---

[22] HyspIRI Ecosystem Spectral Library. Accessed on January 10, 2013: http://hesl.jpl.nasa.gov/

inter-class spectral variability. Remote sensing data with higher spectral resolution and signal-to-noise ratio would also provide higher classification accuracy than that achieved in this study.

Large mapping projects are the driving force behind the development of automated classification tools as they require fast generation of contemporary maps that are consistent and accurate. Such a large-scale project would be the ultimate test determining whether the class-labeling technique has a future or not.

REFERENCES

Adam, E., O. Mutanga, and D. Rugege, 2010. Multispectral and hyperspectral remote sensing for identification and mapping of wetland vegetation: a review. *Wetlands Ecology and Management*, 18 (3): pp. 281 – 296.

Aickin, M., 1990. Maximum likelihood estimation of agreement in the constant predictive probability model, and its relation to Cohen's kappa. *Biometrics*, 46 (2): pp. 293−302.

Aktaruzzaman, A., 2008. Simulation and Correction of Spectral Smile Effect and its Influence on Hyperspectral Mapping. *Master of Science Thesis*, International Institute for Geo-Information Science and Earth Observation, Enschede, Netherlands, 77 pages**.**

Anderson, J.R., 1971. Land-use classification schemes. *Photogrammetric Engineering*, 37 (4): pp. 379–387.

Anggraeni, A., and Lin C., 2011. Application of SAM and SVM Techniques to Burned Area Detection for Landsat TM Images in Forests of South Sumatra. *International Conference on Environmental Science and Technology*, Singapore, 6: pp. V2160 – V2164.

Aplin, P. and P.M. Atkinson, 2004. Predicting missing field boundaries to increase per-field classification accuracy. *Photogrammetric Engineering and Remote Sensing*, 70 (1): pp. 141-149.

Ball, G.H., and D.J. Hall, 1965. ISODATA, a novel method of data anlysis and pattern classification. Technical report NTIS AD 699616. Stanford Research Institute, Stanford, CA.

Ballard, R.J., and L.F. Eastwood, 1977. Estimating Costs and Performance of Systems for Machine Processing of Remotely Sensed Data. *Machine Processing of Remotely Sensed Data Symposium*, 3: pp. 208 – 213.

Ban, Y., 2003. Synergy of Multitemporal ERS-1 SAR and Landsat TM Data for Classification of Agricultural Crops. *Canadian Journal of Remote Sensing*, 29 (4): pp. 518–526.

Barry, P., 2001. *EO-1/Hyperion Science Data User's Guide, Level 1_B*. TRW Space, Defense and Information Systems, Redondo Beach, CA, 60 pages.

Beck L.R., Lobitz B.M., and B.L. Wood, 2000. Remote sensing and human health: new sensors and new opportunities. *Emerging Infectious Diseases*, 6 (3): pp. 217–226.

Behnkre, J., T.H. Watts, B. Kobler, D. Lowe, S. Fox, and R. Meyer, 2005. EOSDIS petabyte archives: tenth anniversary. *Proceedings of 22nd IEEE / 13th NASA Goddard Conference on Mass Storage Systems and Technologies*: pp. 81–93.

Berk, A., L.S. Bernstein, and D.C. Robertson, 1989. MODTRAN: A moderate resolution model for LOWTRAN 7. Air Force Geophysics Laboratory Technical Report GL-TR-89-0122, Hanscom AFB, MA, 38 pages.

Blaes, X., L. Vanhalle, and P. Defourny, 2005. Efficiency of crop identification based on optical and SAR image time series. *Remote Sensing of Environment*, 96 (3–4): pp. 352-365.

Blaschke, T., 2010. Object based image analysis for remote sensing. *ISPRS Journal of Photogrammetry and Remote Sensing*, 65 (1): pp. 2-16.

Boardman, J. W., 1998. Post-ATREM polishing of AVIRIS apparent reflectance data using EFFORT: a lesson in accuracy versus precision. *Summaries of the Seventh JPL Airborne Earth Science Workshop*, Pasadena, CA, USA, 1: page 53.

Bojinski, S., M. Schaepman, D. Schlaepfer, and K. Itten, 2003. SPECCHIO: A spectrum database for remote sensing applications. *Journal of Computers and Geoscience*, 29 (1): pp. 27-38.

Brisco, B., and R.J. Brown, 1995. Multidate SAR/TM synergism for crop classification in western Canada. *Photogrammetric Engineering and Remote Sensing*, 61 (8): pp. 1009–1014.

Campbell, J.B., 1981. Spatial correlation effects upon accuracy of supervised classification of land cover. *Photogrammetric Engineering and Remote Sensing*, 47 (3): pp. 355 – 363.

Castillejo-González, I.L., F. López-Granados, A. García-Ferrer, J. M. Peña-Barragán, M. Jurado-Expósito, M. S. de la Orden, M. González-Audicana, 2009. Object- and pixel-based analysis for mapping crops and their agro-environmental associated measures using QuickBird imagery. *Computers and Electronics in Agriculture*, 68 (2): pp. 207-215.

Cazes, T.A., R.Q. Feitosa, and G.L.A. Mota, 2004. Automatic selection of training samples for multitemporal image classification. *Proceedings of the International Conference on Image Analysis and Recognition* (ICIAR 2004) - Part II, Portugal: 389–398.

Chander, G., and B. Markham, 2003. Revised Landsat-5 TM radiometric calibration procedures and postcalibration dynamic ranges. *IEEE Transactions On Geoscience And Remote Sensing*, 41 (11): pp. 2674 – 2677.

Chapin, F.S.III, E.S.Zavaleta, V.T. Eviner, R.L. Naylor, P.M. Vitousek, H.L. Reynolds, D.U. Hooper, S. Lavorel, O.E. Sala, S.E. Hobbie, M.C. Mack, and S. Diaz, 2000. Consequences of changing biodiversity. *Nature*, 405: pp. 234– 242.

Chavez, P.S., 1988. An improved dark-object subtraction technique for atmospheric scattering correction of multispectral data. *Remote Sensing of Environment*, 24 (3): pp. 459 − 479.

Chen, X., S. Su, J. Wu, and J. Qi, 2009. Making the best use of Landsat MSS images for land use/cover change analysis. *International Conference on Environmental Science and Information Application Technology* (ESIAT), Wuhan, China, 1: pp. 359 – 362.

Cho, M.A., P. Debba, R. Mathieu, L. Naidoo, J.A.N. van Aardt, and G.P. Asner, 2010. Improving discrimination of savanna tree species through a multiple-endmember spectral angle mapper approach: Canopy-level analysis. *IEEE Transactions on Geoscience and Remote Sensing*, 48 (11): pp. 4133-4142.

Christensen, P.R., J.L. Bandfield, V.E. Hamilton, D.A. Howard, M.D. Lane, J.L. Piatek, S.W. Ruff, and W.L. Stefanov, 2000. A thermal emission spectral library of rock-forming minerals. *Journal of Geophysical Research*, 105 (E4): pp 9735–9739.

Cihlar, J., 2000. Land cover mapping of large areas from satellites: status and research priorities. *International Journal of Remote Sensing*, 21 (6 – 7): pp. 1093–1114.

Cihlar, J., Q. Xiao, J. Chen, J. Beaubien, K. Fung, and R. Latifovic, 1998. Classification by progressive generalization: A new automated methodology for remote sensing multichannel data. *International Journal of Remote Sensing*, 19 (14): pp. 2685-2704.

Clark, R.N., A.J. Gallagher, and G.A. Swayze, 1990. Material absorption-band depth mapping of imaging spectrometer data using the complete band shape least-squares algorithm simultaneously fit to multiple spectral features from multiple materials. *In Proceedings of the Third Airborne Visible/Infrared Imaging Spectrometer (AVIRIS) Workshop*, JPL Publication 90-54: pp. 176–186.

Clark, R.N., G.A. Swayze, R. Wise, E. Livo, T. Hoefen, R. Kokaly, and S.J. Sutley, 2007. USGS digital spectral library splib06a. U.S. Geological Survey, *Digital Data Series 231*, http://speclab.cr.usgs.gov/spectral.lib06.

Cochrane, M.A., 2000. Using vegetation reflectance variability for species level classification of hyperspectral data. *International Journal of Remote Sensing*, 21 (10): pp. 2075 – 2087.

Cohen, J., 1960. A coefficient of agreement of nominal scales. *Educational and Psychological Measurement*, 20: pp. 37−46.

Colby, C.P., S. G. Wheeler and W. Miller, 1978. Thematic mapper design parameter investigation. *Proceedings of the Summer Computer Simulation Conference*, Newport Beach, California: pp. 815-823.

Congalton, R. G., and K. Green, 2009. Assessing the accuracy of remotely sensed data: Principles and practice. Boca Raton: CRC Press/Taylor & Francis.

Congalton, R.G., 1991. A review of assessing the accuracy of classifications of remotely sensed data. *Remote Sensing of Environment*, 37: 35–46.

Congalton, R.G., 2001. Accuracy assessment and validation of remotely sensed and other spatial information. *International Journal of Wildland Fire*, 10 (4): pp. 321–328.

Cooley, T.W., G. Anderson, G.W. Felde, M.L. Hoke, and A.J. Ratkowski, 2002. FLAASH, A MODTRAN-4 based atmospheric correction algorithm, its application and validation. *Proceedings of the International Geoscience and Remote Sensing Symposium* (IGARSS), Toronto, ON, Canada, 3: pp. 1414–1418.

Datcu, M., K. Seidel, S. D'Elia and P.G. Marchetti, 2002. Information mining in remote sensing image archives. *ESA Bulletin*, 110: pp. 2923- 2936.

de Carvalho, O.A., and P.R. Meneses, 2000. Spectral Correlation Mapper (SCM): an improvement on the Spectral Angle Mapper (SAM). *NASA JPL AVIRIS Workshop*, 9 pages.

Dennison, P.E., K.Q. Halligan, and D.A. Roberts, 2004. A comparison of error metrics and constraints for multiple endmember spectral mixture analysis and spectral angle mapper. *Remote Sensing of Environment*, 93 (3): pp. 359-367.

Douglas, I. (1999). Hydrological investigations of forest disturbance and land cover impacts in South-East Asia: a review. *Philosophical Transactions of the Royal Society of London*, Series B, 354: pp. 1725–1738.

Draeger, W.C., L.R. Pettenger, A.S. Benson, 1971. The use of small-scale aerial photography in a regional agricultural survey. *Proceedings of the 7th International Symposium on Remote Sensing of the Envoronment*, 2: pp. 1205 – 1217.

Driese, K.L., Reiners, W.A., Merrill, E.H., and K.G. Gerow, 1997. A digital land cover map of Wyoming, USA: a tool for vegetation analysis. *Journal of Vegetation Science*, 8 (1): pp. 133–146.

Duda, R.O., and Hart, P.E., 1973. Pattern classification and scene analysis. Wiley, New York.

Duong, N.D., 2000. Land cover category definition by image invariants for automated classification. *International Archives of Photogrammetry and Remote Sensing*, 33 (B7): pp. 985 – 992.

Eckert, S. and M. Kneubühler, 2004. Application of HYPERION data to agricultural land classification and vegetation properties estimation in Switzerland. *Proceedings of XXth ISPRS Conference*, 12–23 July 2004, Istanbul, Turkey: pp. 866 – 872.

Fisher, P.F., A. Comber, and R. Wadsworth, 2005. Land use and land cover: contradiction or complement. In: Fisher, P.F., and D.J. Unwin (Eds.). *Re-Presenting GIS*, Wiley: pp. 85–98.

Flanders, D., M. Hall-Beyer, and J. Pereverzoff, 2003. Preliminary evaluation of eCognition object-based software for cut block delineation and feature extraction. *Canadian Journal of Remote Sensing*, 29 (4): pp. 441 – 452.

Fleming, M.D., and R.M. Hoffer, 1975. Computer aided analysis of Landsat-1 MSS data: a comparison of three approaches, including a 'modified clustering' approach. Laboratory for Application of Remote Sensing Informations, Note 072475, West Lafayette, Indiana: Purdue University: pp. IB-54 – IB-61.

Foody, G.M., 1992. On the compensation for chance agreement in image classification accuracy assessment. *Photogrammetric Engineering and Remote Sensing*, 58: pp. 1459-1460.

Foody, G.M., 2002. Status of land-cover classification accuracy assessment. *Remote Sensing of Environment*, 80 (1): pp. 185–201.

Foody, G.M., 2008. Harshness in image classification accuracy assessment. *International Journal of Remote Sensing*, 29 (11): pp. 3137−3158.

Foody, G.M., N.A. Campbell, N.M. Trodd, and T.F. Wood, 1992. Derivation and application of probabilistic measures of class membership from the maximum likelihood classification. *Photogrammetric Engineering and Remote Sensing*, 59 (9): pp. 1335 – 1341.

Freidl, M. A., and C. E. Brodley, 1997. Decision tree classification of land cover from remotely sensed data. *Remote Sensing of Environment*, 61: pp. 399 – 409.

Fu, K.S., D.A. Landgrebe, and T.L. Phillips, 1969. Information processing of remotely sensed agricultural data. *Proceedings of the IEEE*, 57 (4): pp. 639 – 653.

Gamon, J. A., H. L. Qiu, D. A. Roberts, S. L. Ustin, D. A. Fuentes, A. Rahman, D. Sims, and C. Stylinski, 1999. Water expressions from hyperspectral reflectance: Implications for ecosystem flux modeling. *In Summaries of the Eighth JPL Airborne Earth Science Workshop*: pp. 9 – 11.

Gates, D.M., H.J. Keegan, J.C. Schleter, and V.R. Weidner, 1965. Spectral properties of plants. *Applied Optics*, 4 (1): pp. 11 – 20.

Gillespie, J.R., 1999. Rationale for a national annual forest inventory program. *Journal of Forestry*, 97 (12): 16 – 20.

Girouard, G., A. Bannari, A. E. Harti, and A. Desrochers, 2004. Validated spectral angle mapper algorithm for geological mapping: Comparative study between quickbird and landsat-TM. *Proceedings of the 20th International Society for Photogrammetry and Remote Sensing (ISPRS) Congress*: Geo-Imagery Bridging Continents, Istanbul, Turkey: pp. 599 – 604.

Goetz, A.F.H., B.N. Rock, and L.C. Rowan, 1983. Remote sensing for exploration; an overview. *Economic Geology*, 78 (4): pp. 573 – 590.

Goetz, A.F.H., 2009. Three decades of hyperspectral remote sensing of the Earth: a personal view. *Remote Sensing of Environment*, 113 (2009): pp. S5 – S16.

Govender, M., K. Chetty, and H. Bulcock, 2007. A review of hyperspectral remote sensing and its application in vegetation and water resource studies. *Water SA*, 33 (2): pp. 145 – 151.

Guerschman, J.P., Paruelo, J.M., Bella, C., Giallorenzi, M.C. and F. Pacin, 2003. Land cover classification in the Argentine Pampas using multitemporal Landsat TM data. *International Journal of Remote Sensing*, 24 (17): pp. 3381 – 3402.

Haralick, R.M., A.H. Christine, Y. Ryuzo, and S.M. Carlyle, 1980. Spectral-temporal classification using vegetation phenology. *IEEE Transactions on Geoscience and Remote Sensing*, GE-18 (2): pp. 167 – 174.

Haralick, R.M., and K. Shanmugam, 1973. Textural features for image classification. *IEEE Transactions on Systems, Man and Cybernetics*, SMC-3 (6): pp. 610 – 621.

Hardin, P.J., and J.M. Shumway, 1997. Statistical significance and normalized confusion matrices. *Photogrammetric Engineering and Remote Sensing*, 63 (6): pp. 735 – 740.

Herold, M., D.A. Roberts, M.E. Gardner, P.E. Dennison, 2004. Spectrometry for urban area remote sensing—Development and analysis of a spectral library from 350 to 2400 nm. *Remote Sensing of Environment*, 91 (3–4): pp. 304 – 319.

Herring, M., T. Chrien, V. Duval, and T. Krabach, 1993. Imaging spectrometry - concepts and system tradeoffs. *Proceedings of the SPIE*, 1874: pp. 11 – 23.

Homer, C.G., R.D. Ramsey, T.C. Edwards Jr, and A. Falconer, 1997. Landscape cover-type modeling using a multi-scene thematic mapper mosaic. *Photogrammetric Engineering and Remote Sensing*, 63 (1): pp. 59 – 67.

Hook, S.J., and M. Rast, 1990. Mineralogic mapping using Airborne Visible Infrared Imaging Spectrometer (AVIRIS), Shortwave Infrared (SWIR) data acquired over Cuprite, Nevada. *Proceedings of the Second Airborne Visible Infrared Imaging Spectrometer (AVIRIS) Workshop*, JPL Publication: pp. 199 – 207.

Huang, Q., G. Wu, J. Chen, H. Chu, 2012. automated remote sensing image classification method based on FCM and SVM. *Proceedings of the 2nd International Conference on Remote Sensing, Environment and Transportation Engineering (RSETE)*, 1-3 June 2012, Nanjing, China: pp.1 – 4.

Hueni, A., J. Nieke, J. Schopfer, M. Kneubuhler, and K.I. Itten, 2009. The spectral database SPECCHIO for improved long-term usability and data sharing. *Computers and Geosciences,* 35 (3): pp. 557-565.

Huth, J., C. Kuenzer, T. Wehrmann, S. Gebhardt, V.Q. Tuan, and S. Dech, 2012. Land cover and land use classification with TWOPAC: towards Automated Processing for Pixel- and Object-Based Image Classification. *Remote Sensing*, 4 (9): pp. 2530 – 2553.

Janssen, L.L.F., and J.D. van Amsterdam, 1991. An object based approach to the classification of remotely sensed images. *Proceedings of the Geoscience and Remote Sensing Symposium*, Espo, Finland, 4: pp. 2191 – 2195.

Jupp, D.L.B., 2001. Discussion around Hyperion data. Office of Space Science and Applications Earth Observation Centre, Canberra, 44 pages.

Kelly, P. M., and White, J.M., 1993. Preprocessing remotely-sensed data for efficient analysis and classification. Knowledge-based systems in aerospace and industry: applications of artificial intelligence. *Proceedings of the SPIE*: pp. 24 – 30.

Khurshid, K.S., K. Staenz, L. Sun, R. Neville, H.P. White, A. Bannari, C.M. Champagne, and R. Hitchcock, 2006. Preprocessing of EO-1 Hyperion Data. *Canadian Journal of Remote Sensing*, 32(2): pp. 84 – 97.

Knorn, J., A. Rabe, V.C. Radeloff, T. Kuemmerle, J. Kozak, P. Hostert, 2009. Land cover mapping of large areas using chain classification of neighboring Landsat satellite images. *Remote Sensing of Environment*, 113 (5): pp. 957 – 964.

Koch, M., J. Inzana, and F. El-Baz., 2005. Applications of Hyperion hyperspectral and aster multispectral data in characterizing vegetation for water resource studies in arid lands. *In The Geological Society of America Annual Meeting*, 37 (7): page 107.

Kokaly, R.F., D.G. Despain, R.N. Clark, and K.E. Livo, 2003. Mapping vegetation in Yellowstone National Park using spectral feature analysis of AVIRIS data. *Remote Sensing of Environment*, 84: pp. 437 – 456.

Kruse F., A. Lefkoff, J. Boardman, K. Heidebrecht, A. Shapiro, P. Barloon, and A. Goetz, 1993. The spectral image processing system (SIPS) - interactive visualization and analysis of imaging spectrometer data. *Remote Sensing of Environment*, 44: pp. 145 – 163.

Kruse, F.A., and S.L. Perry, 2009. Improving multispectral mapping by spectral modeling with hyperspectral signatures. *Journal of Applied Remote Sensing*, 3 (1): pp. 033504 – 033504.

Landgrebe, D., 2000. On the relationship between class definition precision and classification accuracy in hyperspectral analysis. *International Geoscience and Remote Sensing Symposium*, Honolulu, Hawaii: pp. 24 – 28.

Lang, R., G. Shao, B.C. Pijanowski, and R.L. Farnsworth, 2008. Optimizing unsupervised classifications of remotely sensed imagery with a data-assisted labeling approach. *Computers and Geosciences*, 34 (12): pp. 1877 – 1885.

Leite, P.B.C., Feitosa, R.Q., Formaggio, A.R., Da Costa, G.A.O.P., Pakzad, K., and I.D.A. Sanches, 2008. Hidden Markov models applied in agricultural crops classification. *In Proceeding of GEOBIA (GEOgraphic Object-Based Image Analysis for the 21St Century)*, Calgary, Canada.

Lewis, M., V. Jooste, and A. DeGasparis, 2000. Hyperspectral discrimination of arid vegetation. *Proceedings of the 28th International Symposium on Remote Sensing of Environment*, Cape Town, South Africa: pp. 148 – 151.

Lillesand, T.M., and R.W. Kiefer, 2002. *Remote sensing and image interpretation*, Fourth Edition. John Wiley and Sons, New York.

Liu, C.R., P. Frazier, and L. Kumar, 2007. Comparative assessment of the measures of thematic classification accuracy. *Remote Sensing of Environment*, 107 (4): pp. 606 – 616.

Liu, J.Y., D.F. Zhuang, D. Luo, and X. Xiao, 2003. Land-cover classification of China: Integrated analysis of AVHRR imagery and geophysical data. *International Journal of Remote Sensing*, 24 (12): pp. 2485 – 2500.

Lu, D., and Q. Weng, 2007. A survey of image classification methods and techniques for improving classification performance. *International Journal of Remote Sensing*, 28 (5): pp. 823 – 870.

Luc, B., B. Deronde, P. Kempeneers, , W. Debruyn, and S. Provoost, 2005. Optimized Spectral Angle Mapper classification of spatially heterogeneous dynamic dune vegetation, a case study along the Belgian coastline. *The 9th International Symposium on Physical Measurements and Signatures in Remote Sensing*, Beijing.

Lunetta, R.S. and Balogh, M.E., 1999. Application of multi-temporal Landsat 5 TM imagery for wetland identification. *Photogrammetric Engineering and Remote Sensing*, 65 (11): pp. 1303 – 1310.

Ma, Z., and R.L. Redmond, 1995. Tau coefficients for accuracy assessment of classification of remote sensing data. *Photogrammetric Engineering and Remote Sensing*, 61 (4): pp. 435 – 439.

Manakos, I., T. Schneider, and U. Ammer, 2000. A comparison between the ISODATA and the eCognition classification methods on basis of field data. *International Archives of Photogrammetry and Remote Sensing*, 33 (B7): pp. 133 – 139.

Mas, J.F., and I. Ramirez, 1996. Comparison of land use classifications obtained by visual interpretation and digital processing. *International Journal of Applied Earth Observation and Geoinformation*, 3 (4): pp. 278 – 283.

McCaffrey, T.M., and S.E. Franklin, 1993. Automated training site selection for large-area remote-sensing image analysis. *Computers and Geosciences*, 19 (10): pp. 1413 – 1428.

McCormick, C.M., 1999. Mapping exotic vegetation in the everglades from large-scale aerial photographs. *Photogrammetric Engineering and Remote Sensing*, 65 (2): pp. 179 – 184.

Mitchell, J., and N.F. Glenn, 2009. Leafy spurge (*Euphorbia esula* L.) classification performance using hyperspectral and multispectral sensors. *Rangeland Ecology and Management*, 62(1): 16 – 27.

Mozaffar, M.H., M.J. Valadan Zoej, M.R. Sahebi, Y. Rezaei, 2008. Vegetation endmember extraction in Hyperion data. *The International Archives of the Photogrammetry, Remote Sensing and Spatial Information Sciences*, 37 (B7): pp. 409 – 412.

Musy, R.F., R.H. Wynne, C.E. Blinn, J.A. Scrivani, and R.E. McRoberts, 2006. Automated forest area estimation using Iterative Guided Spectral Class Rejection. *Photogrammetric Engineering and Remote Sensing*, 72 (8): pp. 949 – 960.

Mutanga, O., J. van Aardt, L. Kumar, 2009. Imaging spectroscopy (hyperspectral remote sensing) in Southern Africa: an overview. *South African Journal of Science*, 105 (5): pp. 193 – 198.

Nack, M.L., 1977. Rectification and registration of digital images and the effect of cloud detection. *Proceedings of the Machine Processing of Remotely Sensed Data Symposium*, West Lafayette, IN: pp. 12–23.

Næsset, E., 1996. Use of the weighted Kappa coefficient in classification error assessment of thematic maps. *International Journal of Geographical Information Science*, 10: pp. 591−604.

Nangendo, G., A.K. Skidmore, and H. van Oosten, 2007. Mapping East African tropical forests and woodlands — A comparison of classifiers. *Journal of Photogrammetry and Remote Sensing*, 61 (6): pp. 393 – 404.

Oetter, D.R., Cohen, W.B., Berterretche, M., Maiersperger, T.K. and R.E. Kennedy, 2000. Land cover mapping in an agricultural setting using multiseasonal Thematic Mapper data. *Remote Sensing of Environment*, 76: pp. 139 – 155.

Olthof, I., C. Butson, and R. Fraser, 2005. Signature extension through space for northern landcover classification: a comparison of radiometric correction methods. *Remote Sensing of Environment*, 95 (3): pp. 290 – 302.

Ozesmi, S.L., and M.E. Bauer, 2002. Satellite remote sensing of wetlands. *Wetlands Ecology and Management*, 10 (5): pp. 381 – 402.

Pakhale, G.K., and P.K. Gupta, 2010. Comparison of Advanced Pixel Based (ANN and SVM) and Object-Oriented Classification Approaches Using Landsat-7 Etm+ Data. *International Journal of Engineering and Technology*, 2 (4): pp. 245 – 251.

Pal, M., and P. M. Mather, 2005. Support vector machines for classification in remote sensing. *International Journal of Remote Sensing*, 26 (5): pp. 1007 – 1011.

Pal, R., and K. Pal, 1993. A review on image segmentation techniques. *Pattern Recognition*, 26 (9): pp. 1277 – 1294.

Pearlman, J.S., P.S. Barry, C.C Segal, J. Shepanski, D. Beiso, and S.L. Carman, 2003. Hyperion, a space-based imaging spectrometer. *IEEE Transactions on Geoscience and Remote Sensing*, 41(6): pp. 1160 – 1173.

Peddle, D.R., P.H. White, R.J. Soffer, J.R. Miller, and E.F. LeDrew, 2001. Reflectance processing of remote sensing spectroradiometer data. *Computers & geosciences*, 27 (2): pp. 203 – 213.

Peña-Barragán, J.M., K.N. Moffatt, E.P. Richard and S. Johan, 2011. Object-based crop identification using multiple vegetation indices, textural features and crop phenology. *Remote Sensing of Environment*, 115 (6): pp. 1301 – 1316.

Penner, J. E., 1994. Atmospheric chemistry and air quality. In: Meyer, W.B., B.L. Turner II (Eds.), *Changes in land use and land cover: a global perspective,* Cambridge: Cambridge University Press: pp. 175 – 209.

Penuelas, J., I. Filella, C. Biel, L. Serrano, and R. Save, 1993. The reflectance at the 950–970 nm region as an indicator of plant water status. *International journal of remote sensing*, 14(10): pp. 1887 – 1905.

Perry C.H. and M.D. Nelson, 2006. Cartographic standards to improve maps produced by the forest inventory and analysis program. *Proceedings of the Eighth Annual Forest Inventory and Analysis Symposium*: pp. 325 – 331.

Phillips, T.L., 1973. LARSYS User's Manual. Laboratory for Applications of Remote Sensing, Purdue University, West Lafayette, Indiana.

Pontius, R.G., 2000. Quantification error versus location error in comparison of categorical maps. *Photogrammetric Engineering and Remote Sensing*, 66 (8): pp. 1011 – 1016.

Prager, J.M., 1980. Extracting and labeling boundary segments in natural scenes. *IEEE Transactions on Pattern Analysis and Machine Intelligence,* PAMI-2 (1): pp.16 – 27.

Price, J.C., 1994. How unique are spectral signatures? *Remote Sensing of Environment,* 49 (3): pp. 181 – 186.

Rahman, M.M., E. Csaplovics, B. Koch, and M. Kohl, 2004. Interpretation of tropical vegetation using Landsat ETM+ imagery. *International Archives of the Photogrammetry, Remote Sensing and Spatial Information Sciences*: pp. 157 – 162.

Rao, N.R., P.K. Garg, and S.K. Ghosh, 2007. Development of an agricultural crops spectral library and classification of crops at cultivar level using hyperspectral data. *Precision Agriculture*, 8 (4): pp. 173-185.

Roberts, D.A., M. Gardner, R. Church, S. Ustin, G. Scheer, and R.O. Green, 1998. Mapping chaparral in the Santa Monica mountains using multiple endmember spectral mixture models. *Remote Sensing of Environment*, 65 (3): pp. 267 – 279.

Rosenfield, G.H., and K. Fitzpatrick-Lins, 1986. A coefficient of agreement as a measure of thematic classification accuracy. *Photogrammetric Engineering and Remote Sensing*, 52 (2): pp. 223 – 227.

Safavian, S.R., and D. Landgrebe, 1991. A survey of Decision Tree classifier methodology. *IEEE Transactions on Systems, Man, and Cybernetics*, 21 (3): pp. 660 – 674.

Salman, A., M.G. Omran, and A.P. Engelbrecht, 2005. SIGT: Synthetic Image Generation Tool for clustering algorithms. *ICGST International Journal on Graphics, Vision and Image Processing*, 5 (2): pp. 33 – 44.

Schmidt, K. S., and A. K. Skidmore, 2003. Spectral discrimination of vegetation types in a coastal wetland. *Remote Sensing of Environment*, 85 (1): pp. 92 – 108.

Scrivani, J.A., R.H. Wynne, C.F. Blinn, and R.F. Musy, 2001. Phase I forest area estimation using Landsat TM and Iterative Guided Spectral Class Rejection: assessment of possible training data protocols. *Proceedings of the 2nd Annual Forest Service FIA Symposium*, Salt Lake City, Utah: pp. 11 – 14.

Serra, P., Moré, G., Pons, X., 2005. Application of a hybrid classifier to discriminate Mediterranean crops and forests. Different problems and solutions. *Proceedings of the XXII International Cartographic Conference* (ICC 2005), A Coruña, Spain: pp. 1 – 8.

Shafri, H.Z.M., A. Suhaili, S. Mansor, 2007. The performance of Maximum Likelihood, Spectral Angle Mapper, Neural Network and Decision Tree classifiers in hyperspectral image analysis. *Journal of Computer Science*, 3 (6): pp. 419 – 423.

Smith, J.H., S.V. Stehman, J.D. Wickham, and L. Yang, 2003. Effects of landscape characteristics on land-cover class accuracy. *Remote Sensing of Environment*, 84 (3): pp. 342 – 349.

Smits, P.C., S.G. Dellepiane, and R.A. Schowengerdt, 1999. Quality assessment of image classification algorithms for land-cover mapping: a review and proposal for a cost-based approach. *International Journal of Remote Sensing*, 20 (8): pp. 1461 – 1486.

Snedecor, G.W., and W.G. Cochran, 1967. *Statistical methods*. The Iowa State University Press, Ames, Iowa, 593 pages.

Staenz, K, J.W. Schwarz, L. Vernaccini, F. Vachon; C. Nadeau, 1999. Classification of hyperspectral agricultural data with spectral matching techniques. Government of Canada.

Staenz, K., and D.J. Williams, 1997. Retrieval of surface reflectance from hyperspectral data using a look-up table approach. *Canadian Journal of Remote Sensing*, 23 (4): pp. 354 – 368.

Staenz, K., T. Szeredi, and J. Schwarz, 1998. ISDAS - A system for processing/analyzing hyperspectral data. *Canadian Journal of Remote Sensing*, 24 (2): pp. 99 – 113.

Stehman, S.V., 1997. Selecting and interpreting measures of thematic classification accuracy. *Remote Sensing of Environment*, 62 (1): pp. 77 – 89.

Su, W., J. Li, Y. Chen, Z. Liu, J. Zhang, T.M. Low, I. Suppiah, S.A.M. Hashim, 2008. Textural and local spatial statistics for the object-oriented classification of urban areas using high resolution imagery. *International Journal of Remote Sensing*, 29 (11): pp. 3105 – 3117.

Sun, L., R. Neville, and K. Staenz, 2005. Automatic destriping of Hyperion imagery based on spectral moment matching. *Canadian Journal for Remote Sensing*, 34 (S1): pp. S68 – S81.

Swain, P.H., and S.M. Davis, 1978. *Remote Sensing: The Quantitative Approach*. New York: McGraw-Hill: pp. 166 – 174.

Tottrup, C., 2004. Improving tropical forest mapping using multi-date Landsat TM data and pre-classification image smoothing. *International Journal of Remote Sensing*, 25 (4): pp. 717 – 730.

Tou, J.T., and R.C. Gonzalez, 1977. *Pattern Recognition Principles*. Reading MA: Addison-Wesley, 377 pages.

Townshend, J., C. Justice, W. Li, C. Gurney, J. McManus, 1991. Global land cover classification by remote sensing: present capabilities and future possibilities. *Remote Sensing of Environment*, 35 (2–3): pp. 243 – 255.

Van der Meer, F., 2006. The effectiveness of spectral similarity measures for the analysis of hyperspectral imagery. *International Journal of Applied Earth Observation and Geoinformation*, 8 (1): pp. 3 – 17.

Van der Meer, F., 2004. Analysis of spectral absorption features in hyperspectral imagery. *International Journal of Applied Earth Observation and Geoinformation*, 5 (1): pp. 55 – 68.

Van Deusen, P.C., S.P. Prisley, and A.A. Lucier, 1999. Adopting an annual inventory system: User perspectives. *Journal of Forestry*, 97 (12): pp. 11 – 14.

Vogelmann, J.E., Sohl, T., and S.M. Howard, 1998. Regional characterization of land cover using multiple sources of data. *Photogrammetric Engineering and Remote Sensing*, 64 (1): pp. 45 – 57.

Waske, B., and J.A. Benediktsson, 2007. Fusion of Support Vector Machines for classification of multisensor Data. *IEEE Transactions on Geoscience and Remote Sensing*, 45 (12), pp. 3858 – 3866.

Williams, A.P., E.R. Hunt, 2002. Estimation of leafy spurge cover from hyperspectral imagery using mixture tuned matched filtering. *Remote Sensing of Environment*, 82 (2–3): pp. 446 – 456.

Williams, D., V. Myers, and M. Silvious, 2009. Mine classification with imbalanced data. *IEEE Geoscience and Remote Sensing Letters*, 6 (3): pp. 528 – 532.

Xie, Y., Z. Sha, and M. Yu, 2008. Remote sensing imagery in vegetation mapping: a review. *Journal of Plant Ecology*, 1 (1): pp. 9 – 23.

Zha, Y., J. Gao, S. Ni, 2003. Use of normalized difference built-up index in automatically mapping urban areas from TM imagery. *International Journal of Remote Sensing*, 24 (3): pp. 583 – 594.